NAVAL POSTGRADUATE SCHOOL
Monterey, California

THESIS

BACKSCATTER FROM A COMPOSITE ROUGH SURFACE

by

Wilson Banks Decker

December 1980

Thesis Advisor: H. Medwin

Approved for public release; distribution unlimited.

REPORT DOCUMENTATION PAGE

READ INSTRUCTIONS BEFORE COMPLETING FORM

1. REPORT NUMBER	2. GOVT ACCESSION NO.
3. RECIPIENT'S CATALOG NUMBER	
4. TITLE (and Subtitle) Backscatter from a Composite Rough Surface	5. TYPE OF REPORT & PERIOD COVERED Master's Thesis; December 1980
	6. PERFORMING ORG. REPORT NUMBER
7. AUTHOR(s) Wilson Banks Decker	8. CONTRACT OR GRANT NUMBER(s)
9. PERFORMING ORGANIZATION NAME AND ADDRESS Naval Postgraduate School Monterey, California 93940	10. PROGRAM ELEMENT, PROJECT, TASK AREA & WORK UNIT NUMBERS
11. CONTROLLING OFFICE NAME AND ADDRESS Naval Postgraduate School Monterey, California 93940	12. REPORT DATE December 1980
	13. NUMBER OF PAGES 82
14. MONITORING AGENCY NAME & ADDRESS(if different from Controlling Office)	15. SECURITY CLASS. (of this report) Unclassified
	15a. DECLASSIFICATION/DOWNGRADING SCHEDULE

16. DISTRIBUTION STATEMENT (of this Report)

Approved for public release; distribution unlimited.

17. DISTRIBUTION STATEMENT (of the abstract entered in Block 20, if different from Report)

18. SUPPLEMENTARY NOTES

19. KEY WORDS (Continue on reverse side if necessary and identify by block number)

Rough Surface Scattering
Acoustic backscatter
wedge diffraction
boundary wave

20. ABSTRACT (Continue on reverse side if necessary and identify by block number)

Backscatter of acoustic signals generated by surfaces having point scattering and line scattering features is studied experimentally in air. Signals are analyzed for porpagation over three models: a smooth plane wedge, a wedge whose surface is slightly roughened with uniformly-packed lead shot, and one randomly roughened with gravel. Scattering from the rough surfaces at normal incidence is measured to

(20. ABSTRACT Continued)

estimate the statistical parameters that describe the surface roughness. The returned acoustic energy from the composite area of rough surface and wedge for low grazing angles is analyzed to determine whether the identity of the two individual backscatter effects can be separated in their combined spectrum. The near grazing backscattered amplitudes are much larger than predicted by conventional rough surface scattering theory and suggest the presence of a backscattered boundary wave.

Approved for public release; distribution unlimited.

Backscatter from a Composite Rough Surface

by

Wilson Banks Decker
Lieutenant, United States Navy
B.S., United States Naval Academy, 1973

Submitted in partial fulfillment of the
requirements for the degree of

MASTER OF SCIENCE IN ENGINEERING ACOUSTICS

from the

NAVAL POSTGRADUATE SCHOOL
December 1980

ABSTRACT

Backscatter of acoustic signals generated by surfaces having point scattering and line scattering features is studies experimentally in air. Signals are analyzed for propagation over three models: a smooth plane wedge, a wedge whose surface is slightly roughened with uniformly-packed lead shot, and one randomly roughened with gravel. Scattering from the rough surfaces at normal incidence is measured to estimate the statistical parameters that describe the surface roughness. The returned acoustic energy from the composite area of rough surface and wedge for low grazing angles is analyzed to determine whether the identity of the two individual backscatter effects can be separated in their combined spectrum. The near grazing backscattered amplitudes are much larger than predicted by conventional rough surface scattering theory and suggest the presence of a backscattered boundary wave.

TABLE OF CONTENTS

ACKNOWLEDGMENTS

The author acknowledges the invaluable guidance from his thesis advisor, Dr. H. Medwin, of the Naval Postgraduate School. His expertise in experimental analysis and technique has provided the benefits most rewarding from this learning experience.

A special indebtedness is owed to R. Moeller and T. Maris for their superb machining products and useful design suggestions. The assistance offered by K. Smith and J. Brennan through their knowledge of the various electronic equipment and trouble-shooting experience is greatly appreciated. The computer programming efforts of Mrs. Jeanie Savage and Ms. Emily Childs have been most helpful throughout the data analysis.

A special thanks is afforded to my fellow thesis student, Lt. Stephen Hollis, USN, for his collaboration on several experimental aspects and his comaraderie during the tribulations associated with experimental work.

I. INTRODUCTION

Diffraction of acoustic energy from both smooth wedges and rough plane surfaces has been theoretically investigated by a number of authors. Many at sea measurements have been reported for rough surfaces. Of particular interest is the theoretical development of Biot and Tolstoy [1] for impulse diffraction of point source radiation by plane rigid wedges, and the experimental results for sea surface scattering, e.g., Clay and Medwin [2] and Urick [3].

Biot and Tolstoy theory has been tested experimentally by Bremhorst [4] and Spaulding [5] for simple wedges and complex seamount modeling, respectively. The experimental results showed close agreement with theory.

This study continues the experimental comparison of diffraction by various effects in the specific case of backscatter. The approach involved determining the spectral relationship for the smooth wedge and a rigid, random rough surface, separately. A wedge covered with a rough surface of gravel was used to attempt to differentiate between the returned signals from both the wedge and rough surface effects. Also, a wedge covered with lead shot was used to present a uniformly-packed, slightly rough surface. The results were intended to show how the combination of wedge slope angle and surface roughness interact. This relationship would ultimately identify a range of these characteristics

where one signal is not extremely dominant over the other, but rather the two signals could be deconvolved to show their separate effects; and thereby identifying the character of the source of backscatter.

II. RESEARCH FACILITIES

A. ANECHOIC CHAMBER

The experiments were conducted in the Naval Postgraduate School anechoic chamber (air), which provides excellent isolation from external noise sources, absorption of internal sounds, and atmospheric stability. The internal design of Fiberglas wedges allows for absorption of approximately 99% of the incident sound of frequencies greater than 100 Hz.

B. DATA PROCESSING EQUIPMENT

Data acquisition and processing were accomplished by using a digital computer system composed of four major components interfaced to provide high speed analog to digital conversion, digital processing, and data printout. The design was developed by the Special Projects section of Naval Air Development Center in conjunction with Pinkerton Computer Consultants, Inc., of Warminster, Pennsylvania. The major components are:

1. Interdata Model 70 Computer

This minicomputer is a digital design that is FORTRAN and BASIC programmable with a 64 thousand byte memory. Additionally, data stored on floppy discs or digital tape cassettes can be input for processing.

2. Phoenix Analog to Digital Converters, Model ADC 912

Two ADC 912 analog to digital converters may be used separately or simultaneously. Each converter is a high

speed, high accuracy device capable of encoding ±10 volt input signals into twelve binary bits of data with a resolution limit of one part in 4,095 at a maximum rate of 2 microseconds per conversion. It measures the input voltage relative to an internal precision reference voltage with an accuracy of ±0.025% of full range. The ADC 912's will accommodate a typical commutating through-put rate of 476,190 channels per second, including settling time. The sampling frequency is set in a stable frequency oscillator and sent to the converters via a sampling circuit. As used conservatively at NPS, the maximum sampling frequency is 320,000 Hz.

3. Orbis Diskette Drive, Model 76S

The Model 76S diskette drive is a peripheral device interfaced with the Interdata 70 Minicomputer in order to read and write on an industry standard floppy disc. The dual drive unit provides 3.2 million bits of data with a data rate of 250,000 bits per second encoding for each drive and is capable of a 6 millisecond access time track-to-track.

4. Texas Instruments Silent Electronic Data Terminal, Model 733

The TI 733 consists of a keyboard used as a programming input/output control device, a printer, and transmit/receive mechanism for the peripheral disc drive unit. The overall system facilitates rapid, accurate processing of any desired type of analog electrical signal and was used primarily for frequency domain analyses using standard FFT algorithms.

C. STANDARD EQUIPMENT LIST

The following scientific equipment was utilized to conduct the experimental work:

Interface Technology Timing Simulator/Word Generator, Model RS-648

Wavetek Arbitrary Waveform Generator, Model 175

Instruments, Inc., Power Amplifier, Model L2

E&L Instruments DD-1 Digi Designer

Tektronix Type 551 Oscilloscope with two dual-trace plug-in units

General Radio Type 1312 Coherent Decade Oscillator

Hewlett-Packard Electronic Counter, Model 5223L

Fluke Digital Multimeter, Model 8000A

Hewlett-Packard DC Power Supply, Model 721A (two)

Princeton Applied Research Pre-Amplifier, Model 113 (two)

Krohn-Hite Frequency Filter, Model 3550

Bruel and Kjaer Type 4145 Condenser Microphone

Bruel and Kjaer Type 4133 Condenser Microphone

Bruel and Kjaer Microphone Preamplifier, Model 2619

Bruel and Kjaer Microphone Power Supply, Model 2804

The equipment diagram for the experiment is shown in Figure 3.

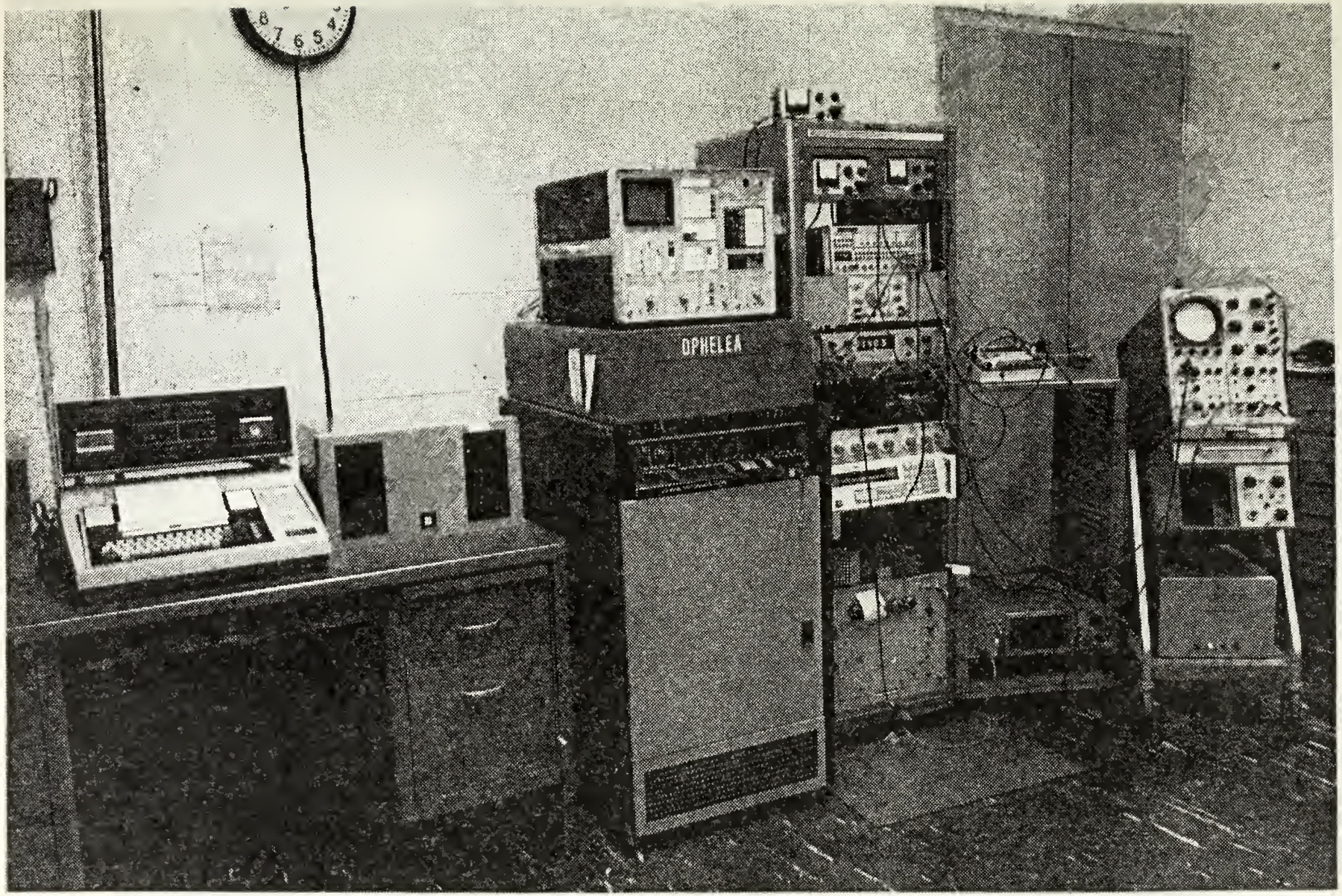

Figure 1. Laboratory Processing System

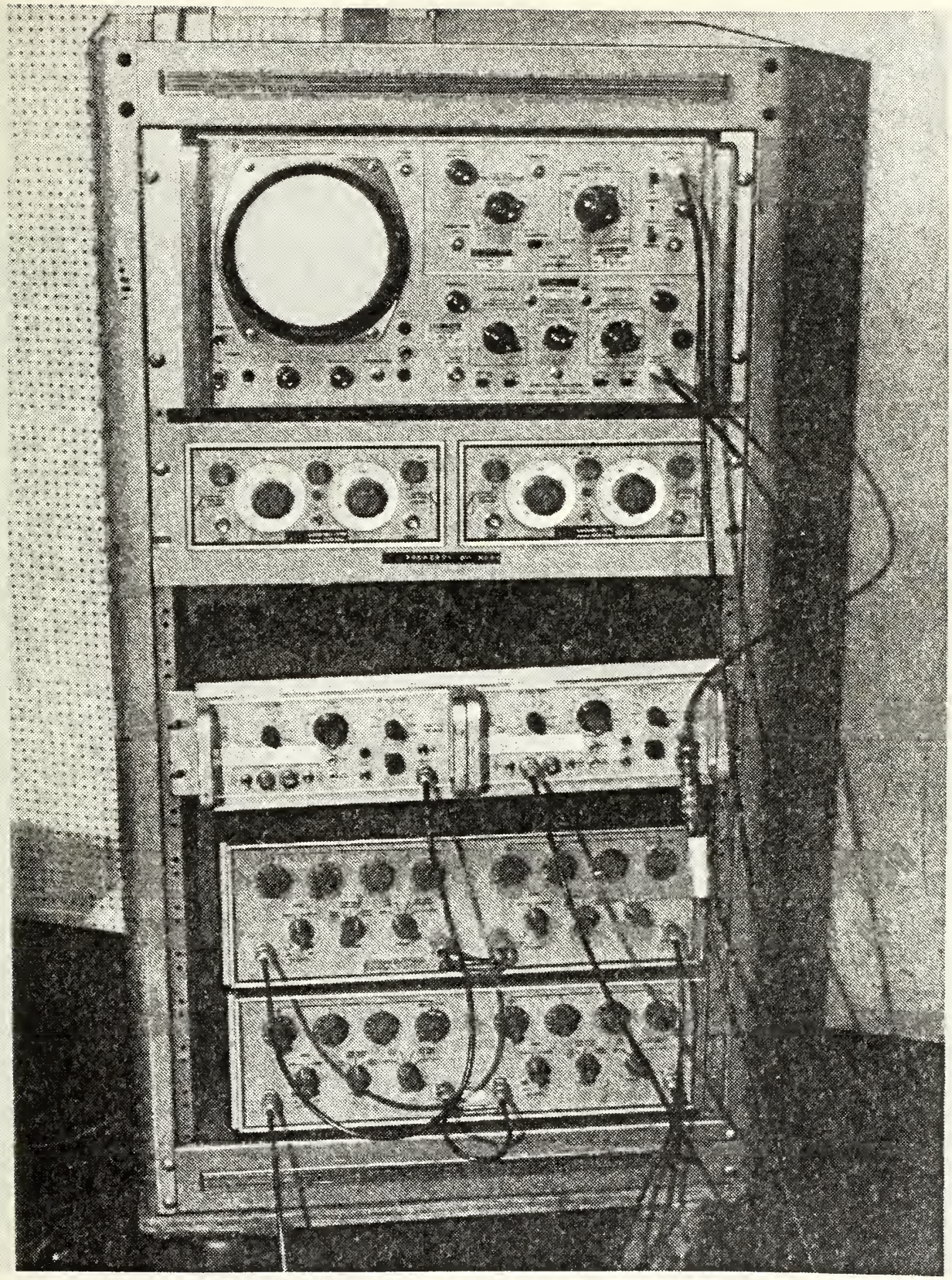

Figure 2. Typical Rack Mounting

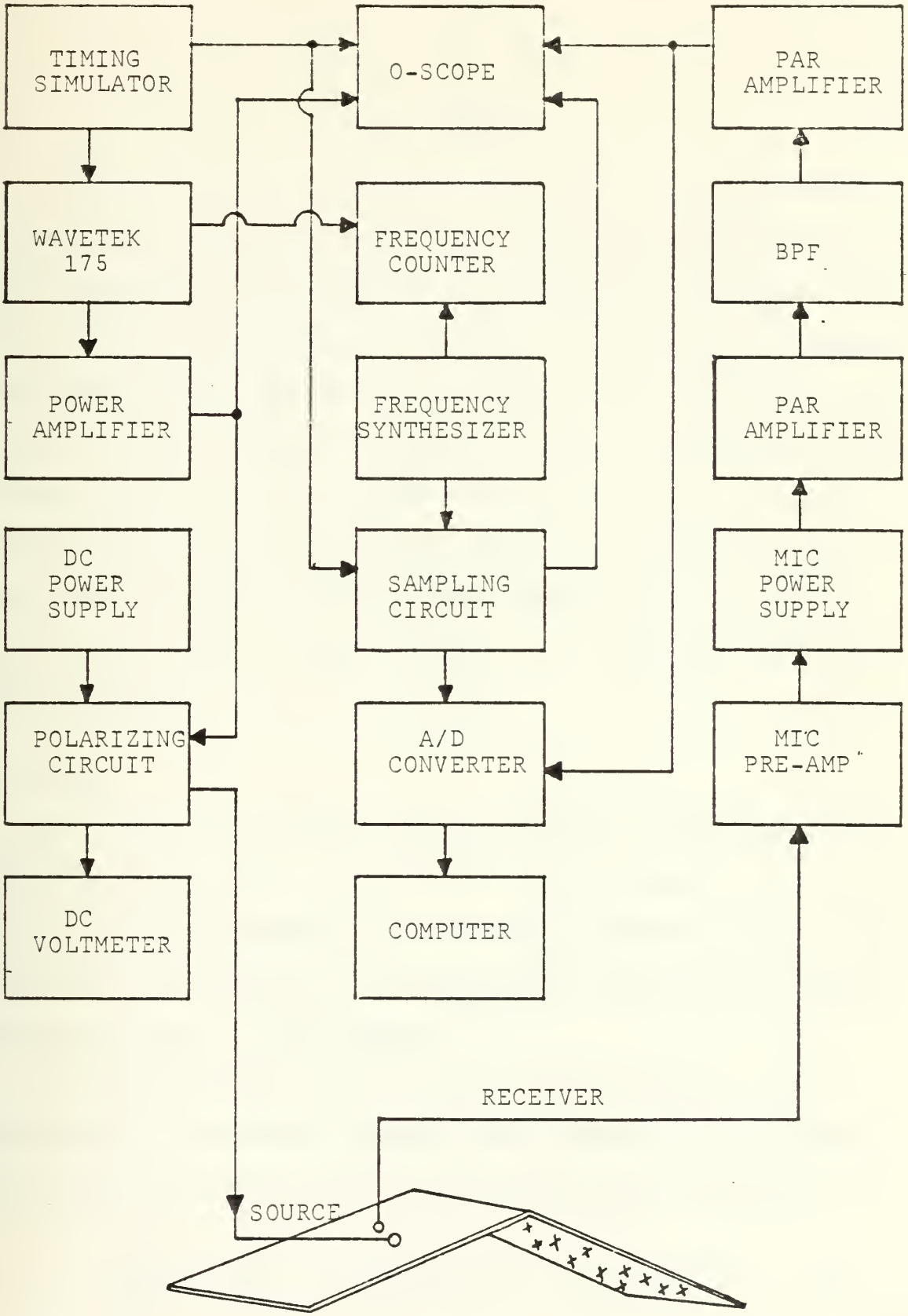

Figure 3. Equipment Diagram

III. THEORY

Scattering can be generally explained as the phenomenon which occurs whenever a wave front encounters an obstacle, thus producing a new source by the principle of Huygens wavelets. With the exception of forward scatter, we can separate the sound waves scattered by an object from the direct sound wave by using a pinging technique and observing the scattered signal when there is no signal from the source [2]. This experimental work involves the study of two theories for backscatter--that for which sound impinges on a change of slope such as for a wedge and that for sound scatter from a rough surface.

A. WEDGE

To examine the former theory, consider the model of an infinite wedge which is bounded by rigid plates at $\theta = 0$, $\theta = \theta_w$ and intersecting along the apex, chosen as the z-axis. The region is occupied by a homogeneous compressible fluid of sound speed, c, and density, ρ.

To determine the normal modes of the system, it is convenient to solve the acoustic wave equation in cylindrical coordinates, in terms of the displacement potential ϕ:

$$\frac{\partial^2\phi}{\partial r^2} + \frac{1}{r}\frac{\partial\phi}{\partial r} + \frac{1}{r^2}\frac{\partial^2\phi}{\partial\theta^2} + \frac{\partial^2\phi}{\partial z^2} = \frac{1}{c^2}\frac{\partial^2\phi}{\partial t^2} \qquad (1)$$

The harmonic solutions to this equation are of the form

$$\phi(r,\theta,z,t) = e^{\pm i\nu\theta} H_{\nu}^{(1,2)}(\kappa r) e^{\pm i\gamma z} e^{\pm i\omega t} \qquad (2)$$

where ν, κ, and γ are separation constants and may be thought of as components of the wave propagation vector, k, in the azimuthal, radial, and z directions, respectively, and

$$\gamma^2 = \frac{\omega^2}{c^2} - \kappa^2 \; . \qquad (3)$$

Boundary conditions can be established such that the sides of the wedge are assumed to be perfectly rigid, requiring the displacements normal to the sides to vanish, and can be expressed mathematically as,

$$\frac{\partial \phi}{\partial \theta} = 0 \quad \text{at} \quad \theta = 0, \; \theta = \theta_W \; . \qquad (4)$$

Writing the first term of the RHS of equation (2) as

$$e^{\pm i\nu\theta} = \cos \nu\theta + \sin \nu\theta$$

and applying the boundary conditions yields the solution to equation (1),

$$\phi = \cos \nu_n\theta \; H_{\nu}^{(1,2)} \; e^{\pm i\gamma z} \; e^{\pm i\omega t} \qquad (5)$$

where

$$\nu_n = \frac{n\pi}{\theta_W} . \tag{6}$$

At r = 0, the imaginary part of the Hankel function becomes infinite, which is not physically realizable. Therefore, only the real parts of $H_\nu^{(1,2)}$, which are Bessel functions of the first kind, will be kept.

Biot and Tolstoy [1] develop this theory by assuming an explosive point source at r_0, θ_0, and z = 0, which leads to solutions to equation (5) that are symmetric in the z-axis. Applying the method of normal coordinates, they arrive at the solution,

$$\frac{\partial \theta}{\partial t} = -\frac{c}{\theta_W} \sum_n \cos \nu_n \theta \cos \nu_n \theta_0 \, I_n , \quad ct \geq z \tag{7}$$

where

$$I_n = \int_0^\infty J_{\nu_n}(\kappa r) J_{\nu_n}(\kappa r_0) J[\kappa (c^2 t^2 - z^2)^{1/2}] \kappa \, d\kappa \tag{8}$$

For a detailed look at the mathematics of the solution technique, see Refs. 1 and 6. A transform given in Appendix X of Ref. 6 may be used to reduce I_n to more physically comprehensible terms.

Now let

$$t_0 = \frac{1}{c}[(r - r_0)^2 + z^2]^{1/2} \tag{9}$$

$$t' = \frac{1}{c}[(r + r_0)^2 + z^2]^{1/2}$$

where t_0 is the least possible time required for a sound pulse to travel directly from a source to receiver and t' is the time required to travel from source to wedge apex to receiver. Equation (8) will have three solutions: $t < t_0$, $t_0 \leq t \leq t'$, $t' \leq t$. For $t < t_0$, $I_n = 0$ as would be expected and there is no signal. For $t_0 \leq t < t'$, the solution describes the acoustic field for the direct energy (not of interest), reflected energy, and any backscattered energy prior to the signal from the wedge apex (for the rough surface case considered). For $t' \leq t$, the solution is the one of interest for the theory applied to backscatter from wedges.

For this case,

$$I_n = - \frac{1}{\pi r r_0 \sinh y} \sin \nu_n \pi \, e^{-\nu_n y} \qquad (10)$$

where

$$y = \text{arc cosh} \frac{c^2 t^2 - (r^2 + r_0^2 + z^2)}{2 r r_0} \qquad (11)$$

Using this solution, equation (7) becomes

$$\frac{\partial \phi}{\partial t} = \frac{c}{\pi \theta_W} \frac{1}{r r_0 \sinh y} \sum_n \cos \nu_n \theta_0 \cos \nu_n \theta \sin \nu_n \pi e^{-\nu_n y}, \qquad (12)$$

$$t' < t$$

Rewriting the trigonometric functions in terms of their exponential identities and then collecting the conjugate pairs, equation (12) is rewritten as

$$\frac{\partial \phi}{\partial t} = \frac{c}{4\pi\ \theta_W} \frac{1}{r\ r_0\ \sinh\ y} e^{-\pi y/\theta_W} \cdot \left[\frac{\sin(\pi/\theta_W)(\pi \pm \theta \pm \theta_0)}{1-2e^{-\pi y/\theta_W} \cos(\pi/\theta_W)(\pi \pm \theta \pm \theta_0) + e^{-2\pi y/\theta_W}}\right] \tag{13}$$

when the ± signs indicate that the term in brackets is actualy a sum of four terms corresponding to all possible combinations of these signs.

For the unit impulse source used in Refs. 1 and 6, the displacement potential ϕ is related to the acoustic pressure by

$$p = -\rho \frac{\partial^2 \phi}{\partial t^2} \tag{14}$$

If, on the other hand, one assumes a source that is a delta function in time as well as space, the acoustic pressure resulting from the backscattered wave alone is given by

$$p = \frac{-\rho\ c}{4\pi\ \theta_W} \frac{1}{r\ r_0\ \sinh\ y} e^{-\pi y/\theta_W} \cdot \left[\frac{\sin(\pi/\theta_W)(\pi \pm \theta \pm \theta_0)}{1-2e^{-\pi y/\theta_W} \cos(\pi/\theta_W)(\pi \pm \theta \pm \theta_0) + e^{-2\pi y/\theta_W}}\right] \tag{15}$$

where

$$y = \text{arc cosh} \frac{c^2t^2 - (r^2 + r_0^2 + z^2)}{2\, r\, r_0}$$

and

θ_W = fluid filled region above the wedge

θ_0 = angle between the wedge side and the source

θ = angle between the wedge side and the receiver

r_0 = distance from source to wedge crest

r = distance from wedge crest to receiver

z = distance along wedge crest measured from point of intersection of least time travel path

See figure 4 for illustration of geometry.

The backscattering process can be described as follows. A point source at a distance r_0 from the wedge crest transmits a spherical wavefront. The wavefront first impinges the crest along the least time travel path at time, $t = r_0/c$. The wavefront then continues to arrive at progressively later t along increasing distance z. This in effect produces a continuous series of point sources along the crest which reradiate. Thus the crest of the wedge acts as a line source with time shading along the line.

Since the frequency domain solution to the impulse wave scattering problem is more familiar to the applied acoustician,

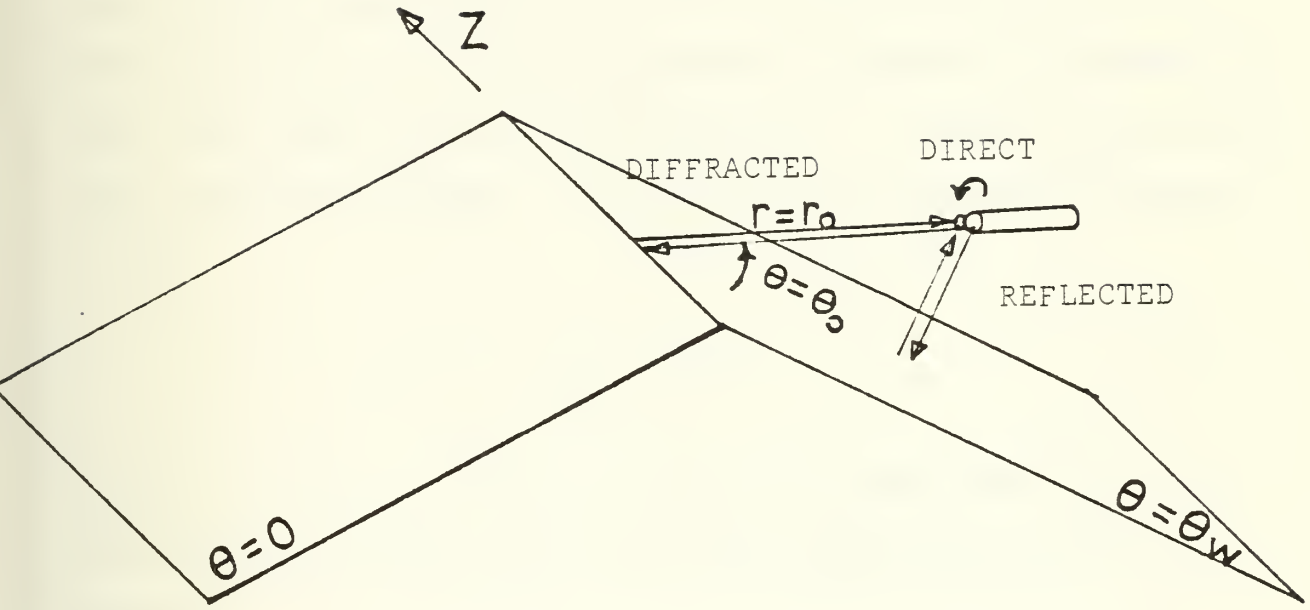

Figure 4. Typical wedge geometry

equation (15) has been transformed to the frequency domain by Medwin [7], and the computed theoretical values have been compared to experimental data.

B. ROUGH SURFACE SCATTER

The statistical approach to the scattering theory describes the random surface by the distribution of its surface heights about a mean level and by a correlation function that relates the heights at various points on the surface. The distribution of surface heights is assumed to be Gaussian with zero mean and standard deviation, σ, which is identically the rms surface height. The correlation function is assumed to be

$$C(\tau) = \exp -(\tau/L)^2 \qquad (16)$$

where L is the correlation distance of the surface and τ is the distance between any two points whose correlation is desired.

The derivation of this theory is given by Beckmann and Spizzichino [8] for electromagnetic radiation. However, acoustic scattering is analagous to electromagnetic, where the pressure field is developed by using the Helmholtz integral and applying boundary conditions in conjunction with the Kirchhoff approximation [2]. The further assumption that the incident pressure is constant over a rectangular insonified area and zero elsewhere is imposed to yield

a formula for the scattered pressure from a random rough surface,

$$p_2 = p_{20} \frac{F}{A} \int\int e^{i\vec{v}\cdot\vec{r}}\, dxdy \qquad (17)$$

p_{20} = specular scatter from smooth surface

$$p_{20} = \frac{i\, k\, p_{10}\, A \cos\theta_1}{2\pi r_2} \exp(ikr_2) \qquad (18)$$

p_{10} = incident pressure

θ_1 = angle of incidence

θ_2 = angle of scatter to receiver

r_2 = range from surface to receiver

$$F = \frac{1 + \cos\theta_1 \cos\theta_2 - \sin\theta_1 \sin\theta_2 \cos\phi}{\cos\theta_1(\cos\theta_1 + \cos\theta_2)} \qquad (19)$$

$\vec{v}$ = propagation wave vector, a function of geometry.

Since p_2 is a complex quantity, the mean square scattered pressure $\langle p_2 p_2^* \rangle$ must be calculated in order to introduce the scattered intensity. This then is related to the mean and variance of the scattered pressure by the expression

$$\langle p_2 p_2^* \rangle = \langle p_2 \rangle \cdot \langle p_2^* \rangle + \mathrm{Var}[p_2] \,. \qquad (20)$$

The mean scattered pressure is equivalent to the coherent component of the specularly scattered pressure field since it has constant phase with respect to the smooth reflected pressure.

$$\langle p_2 \rangle = p_{20} F \exp(-g/2) \operatorname{sinc} v_x X \operatorname{sinc} v_y Y \quad (21)$$

where

$$\operatorname{sinc} v_x X = \frac{\sin v_x X}{v_x X}$$

and g is defined as the roughness parameter,

$$g = k^2 \sigma^2 (\cos \theta_1 + \cos \theta_2)^2 . \quad (22)$$

The variance is derived by assuming surface roughness to be isotropic,

$$\mathrm{Var}[p_2] = \frac{\pi F^2 L^2 \exp(-g) p_{20}^2}{A} \cdot \sum_{m=1}^{\infty} \frac{g^m}{m m!} \exp\left[\frac{-(v_x^2 + v_y^2) L^2}{4m}\right] \quad (23)$$

and this equates to the incoherent component of the scattered pressure field. A more detailed analysis of the mathematics in this section can be found in Ref. 8.

For the specular case, the scattered intensity reduces to

$$\frac{\langle p_2 p_2^* \rangle}{|p_{20}|^2} = \exp(-g) + \frac{\pi L^2}{A}\left[\exp(-g) \sum_{m=1}^{\infty} \frac{g^m}{mm!}\right] \quad (24)$$

The expression in brackets is defined as S(g), and approaches a constant linear slope at very low or very high values of roughness,

$$S(g) \rightarrow g \quad \text{for} \quad g < .1$$

$$S(g) \rightarrow 1/g \quad \text{for} \quad g > 10 .$$

For normal incidence, the relative scattered intensity shows a relationship to frequency squared through e^{-g} for $g < 1$ and approaches an asymptotic value of $AL^2/2\sigma^2 r^2$ for $g > 10$.

In the backscatter case, a surface backscattering factor is defined as

$$S_B = \frac{\langle p_2 p_2^* \rangle}{|p_1|^2} \cdot \frac{r_2^2}{A} \quad (25)$$

where p_1 is the incident pressure at the surface. For a relatively smooth surface, $g << 1$, the intensity becomes

$$\langle p_2 p_2^* \rangle = \frac{16 \pi^2 L^2 \sigma^2 p_{20}^2}{\lambda^2 \cos^2 \theta_1 \, A} \exp(-k^2 L^2 \sin^2 \theta_1 - g) . \quad (26)$$

and the backscattering factor is

$$S_B = \frac{16\pi^3 L^2 \sigma^2}{\lambda^4} \exp(-k^2 L^2 \sin^2\theta_1 - g) \quad . \qquad (27)$$

For the rough surface, $g >> 1$, the coherent term is considered negligible so that the variance equals the intensity

$$\langle p_2 p_2^* \rangle = \mathrm{Var}[p_2] = \frac{\pi F^3 p_{20}^2 L^2}{Ag} \exp[-(v_x^2 + v_y^2) L^2/4g] \qquad (28)$$

and the backscattering factor becomes

$$S_B = (8\pi\varepsilon^2 \cos^4\theta_1)^{-1} \exp[-\tan^2\theta_1/2\varepsilon^2] \qquad (29)$$

where

$$\varepsilon^2 = \frac{2\sigma^2}{L^2} = \text{mean square slope} \quad . \qquad (30)$$

IV. EXPERIMENTAL DESIGN AND PROCEDURES

A. DESIGN OF THE MODELS

The choice of models to experimentally test the theory was a progression from a simple wedge to more complex roughened surfaces and finally to a combination of these two features. It was necessary that the models appear to the source and receiver as being spatially infinite compared to the wavelength of the signals. By using sufficiently large model dimensions and a pulsed signal technique, interference from edge diffraction was avoided and the surface could be considered infinite for the frequency band of the experiment. Additionally, the models were required to approximate a perfectly rigid condition. Aluminum was selected for the building material due to its availability, machinability, rigidity, and reflection coefficient in air of almost unity.

1. Smooth Wedge

The wedge fabricated for Spaulding's [5] experimental work was available and appropriate for this part of the study. The dimensions--two pieces of 1/4" thick aluminum, each 1.52 m. (5 ft.) long by 0.6 m. (2 ft.) wide, joined at the crest forming an interior angle of 152°--were dictated by the size of an aluminum section available, which satisfied the infinite surface criterion. The symmetrical angle of 14° with the horizontal was chosen to approximate the average upslope and downslope of the seamount modeled by Spaulding. For

this study of backscatter, the wedge presented a depression angle of 28° as the sound wave traveled up the slope and encountered the effect from the crest.

2. Rough Surface

The rough wedge design required a random surface whose rms height and rms slope of roughness were known parameters for comparison to theory. Since the final model was to be a combination of a wedge and rough surface, the rough surface was prepared on a model of identical dimensions as those for the smooth wedge. Due to weight and cost, aluminum of 3/16" thickness was chosen, yet the massiveness was maintained by the addition of lead shot as the roughening element. Since the wedge had a dual use with another experimental study, lead shot was chosen to be compatible for both experiments and was distributed uniformly in a dense packing pattern over the surface. It was intended that the frequency range of the study be $kh < 1$ where h is the separation of the shot so that the regularity of the uniform packing would not affect the backscatter.

However, for the wavelengths available (due to the $kh < 1$ limitation), the size of the lead shot and the uniform packing presented a surface that appeared "acoustically smooth" i.e., $g < 1$. Furthermore, since the theory for a random rough surface assumed Gaussian distribution for the roughness, a different roughening element was required to approximate this distribution. The wedge-shaped base remained

the same with gravel applied to roughen the surface. The statistical quantities of this surface were determined from height measurements by Lt. E. Jordan.

B. SOURCE/RECEIVER SELECTION

Bremhorst [4] conducted extensive experimental testing to determine the most suitable source and receiver to satisfy the requirements of size, frequency response, acoustic output, and receiver sensitivity. After a compromise of these parameters for the best experimental combination, Bruel and Kjaer (B&K) condenser microphones were chosen as both source and receiver.

To examine the Biot-Tolstoy theory, it is desirable to approximate a point source to transmit spherically symmetrical waves. This condition requires that the source dimensions be smaller than the wavelength of the transmitted signal ($ka << 1$, where k is the wave number and a is the radius of the source). To approach the assumption of a point source, the smallest possible microphone should be used as a source; however, the limiting factor for size is the need for a usable acoustic pressure output over the frequency range of interest. This was especially critical when transmitting over the rough surface, as the effects of secondary scatter added to the transmission loss. Although the B&K condenser microphones operate as piston radiators, they follow the fundamental property of radiating a spherical diverging wave but with a directivity factor included. The

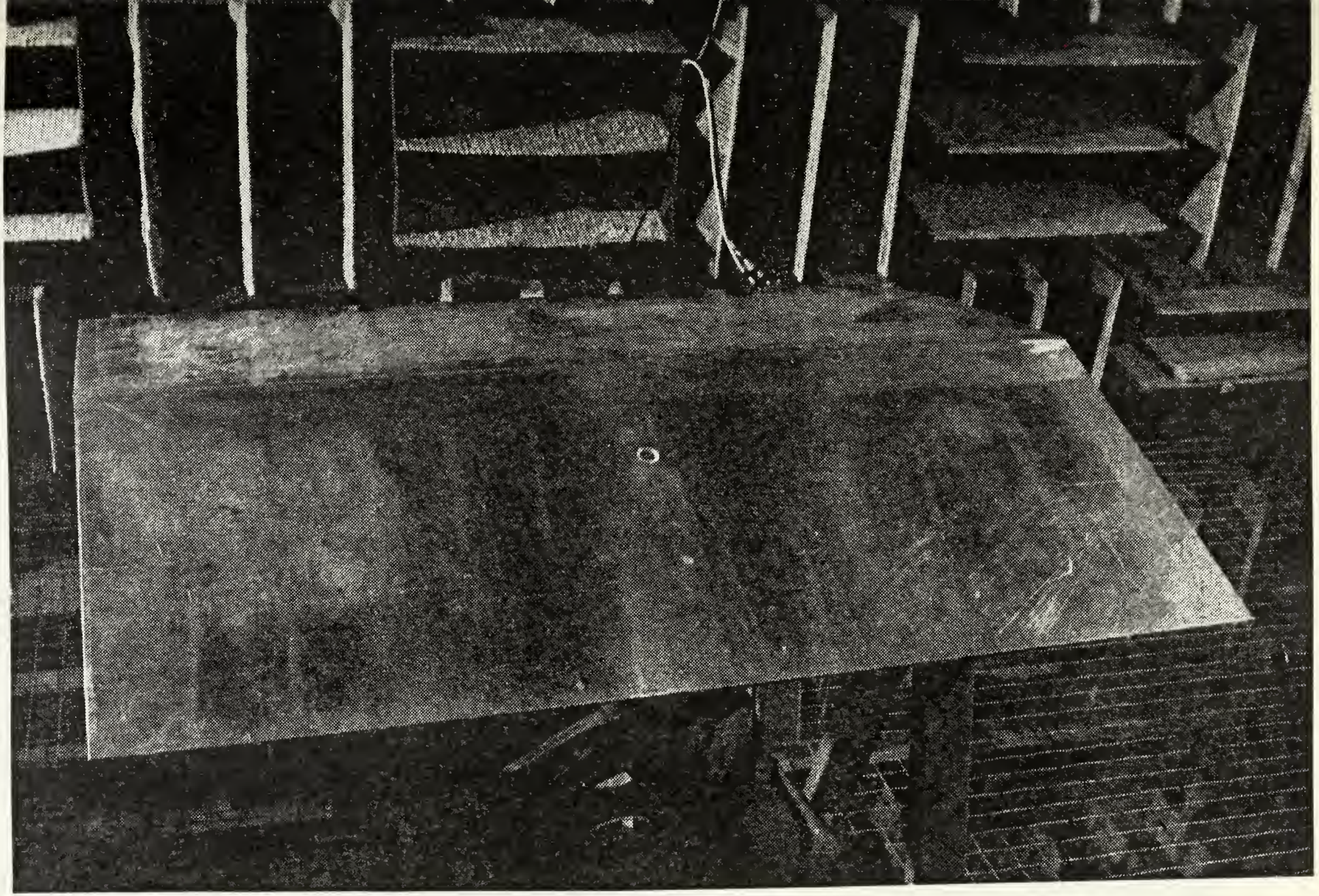

Figure 5. Smooth wedge with source-receiver suspended

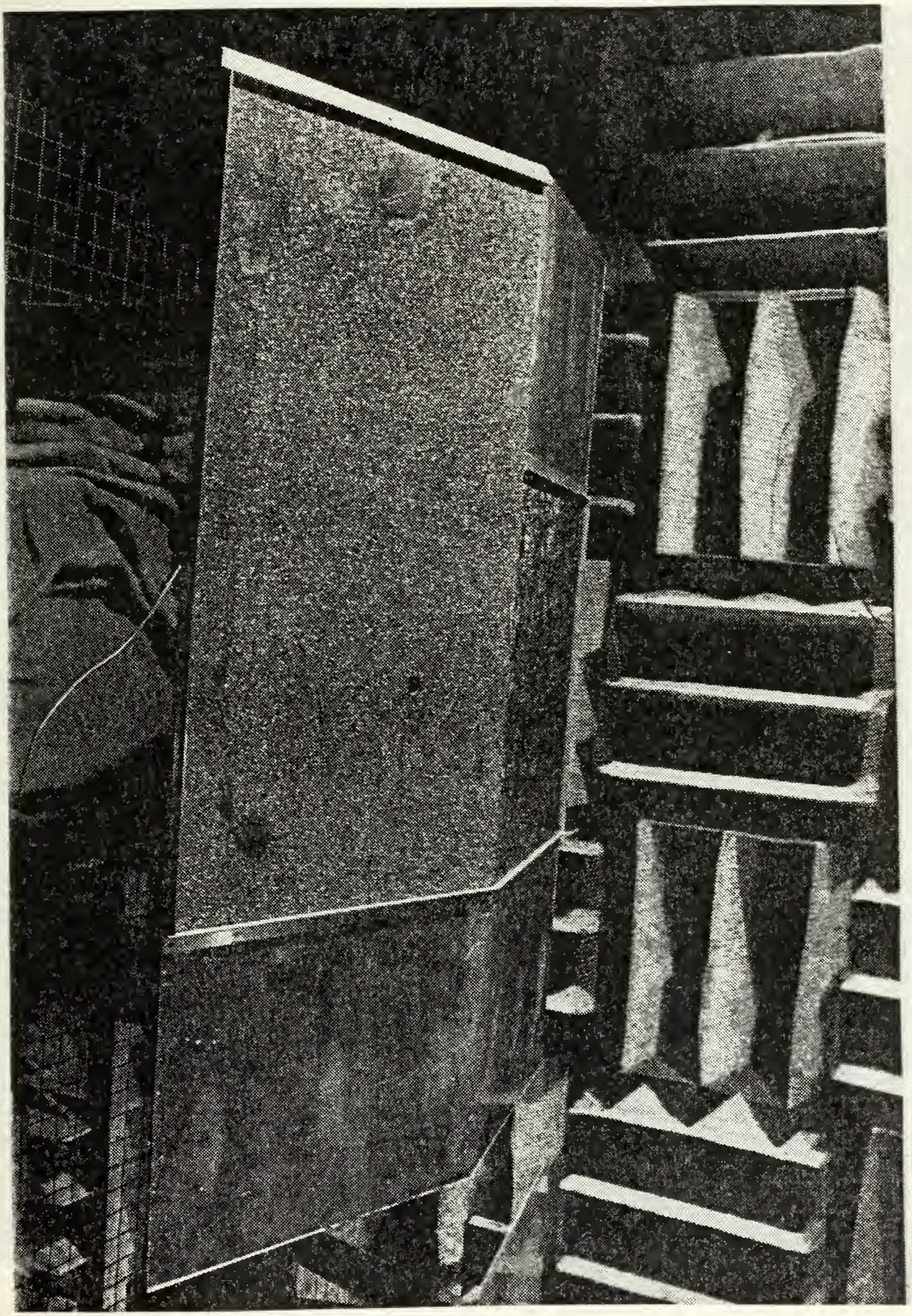

Figure 6. Wedge covered with lead shot

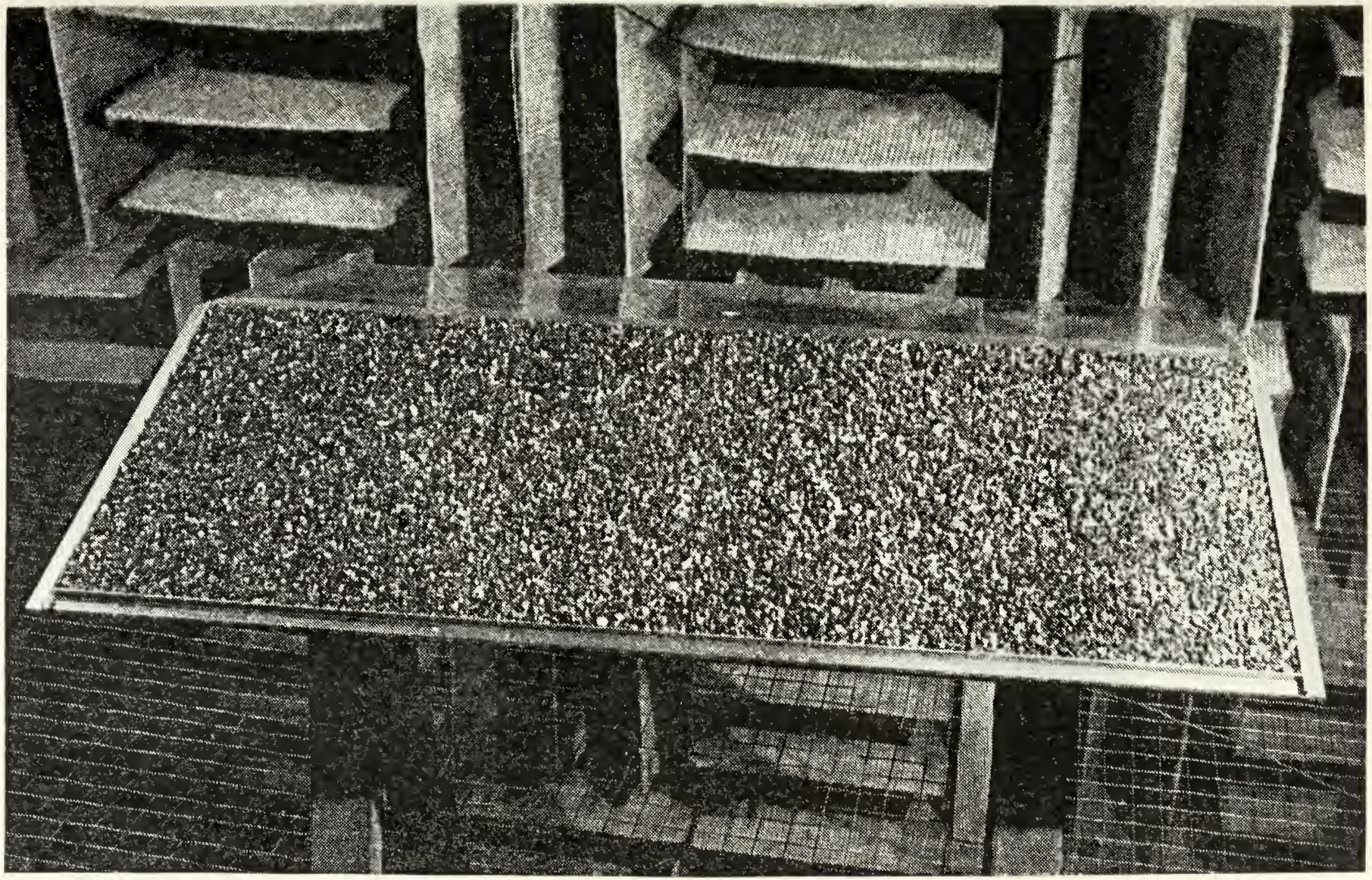

Figure 7. Wedge with gravel rough surface

directivity term could be ignored as long as the sound field was essentially constant over the insonified area of interest, i.e., on or near the acoustic axis of the microphone.

The receiver selection involved the trade-off between the smallest possible microphone for good high frequency response and the largest receiver to maintain a sensitivity level sufficient to detect the weak, returned signals. The optimum combination was using the 1" B&K 4145 as the source and the 1/2" B&K 4133 as the receiver.

Another important consideration was that the pulse length of the single-ping signal determined the resolution of the surface roughness that could be recognized. The B&K condenser microphone exhibited the disadvantage of transforming a single-ping waveform into a repetitive periodic waveform decaying with time, or a "ringing" effect. The result was a larger area of insonification than desired because of the increased time of the output signal.

This study embarked on the task of constructing and testing an alternate microphone that could generate the required acoustic power while maintaining receiver sensitivity, yet reduce or remove any ringing effect. A solid dielectric Mylar transducer was designed using the guidelines of Ref. 9. Four transducers were fabricated--two 3" and two 1", with each size having different degrees of roughness of the backplate. It was projected that if these designs decreased the

ringing effect, a newer material of polyvinylidene fluoride (PVF_2) could replace the Mylar surface to further enhance the output capability and the receiver sensitivity. This material has the advantage of being prepolarized to allow more electrical signal to either generate or detect the acoustic signal.

Testing indicated that the Mylar and PVF_2 dielectric transducers also showed a ringing effect, so that three additional tests were conducted to compare the amplitudes and duration of received signal of all the transducers. A common source was used to radiate to the various receivers, and likewise a common receiver was used to compare the transducers as sources. The sources and receivers were facing each other on their respective acoustic axes. The third test used a common receiver with the various sources, but compared the reflected signal due to normal incidence on a rigid plate (Table 1).

A 3" Mylar transducer was used as a common source with the resulting differences in receiver characteristics being greater than any of the other tests. The 1" B&K microphone (source) had a signal strength 23-29 dB greater than any of the dielectric transducers, but demonstrated a ringing of 600 microseconds that was from two to four times longer than the others.

With an 1/8" B&K microphone as a common receiver, the sources were more similar in their results. The 3" Mylar

Table 1

Transducer Comparison--All values determined from oscilloscope photos

A. 3" Mylar source

RCVR	AMPLITUDE [dB re 1v]	DURATION [μsec]
1/8" B&K	-18.4	150
1/2" B&K	- 1.4	300
1" B&K	0.8	600
1" PVF_2	-22.0	300
1" Mylar	-28.0	200
3" Mylar	-24.4	150

B. 1/8" B&K receiver

SOURCE	AMPLITUDE [dB re 1v]	DURATION [μsec]
1/2" B&K	-16.5	50
1" B&K	-14.0	100
1" PVF_2	-16.5	50
1" Mylar	-14.0	40
3" Mylar	-10.5	25

C. Reflection off smooth, rigid plate at normal incidence; 1/2" B&K receiver

SOURCE	AMPLITUDE [dB re 1v]	DURATION [μsec]
1" B&K	- 3.1	180
1" PVF_2	-18.8	160
1" Mylar	-18.4	120
3" Mylar	-26.0	100

Note: "Duration" is measured from onset of signal to time when noise is greater than signal.

transducer had a 6 dB stronger signal than the 1/2" B&K and the 1" PVF_2 and was 4 dB stronger than the 1" B&K and the 1" Mylar. Only a small variation in the ringing existed where the 3" Mylar signal duration was 25 microseconds as compared to the 1" B&K of 100 microseconds.

The reflected signal indicated that the 1" B&K source signal exceeded those of the dielectrics by 15 to 23 dB, yet the ringing of 180 microseconds duration was only slightly more than the best case of 100 microseconds for the 3" Mylar.

These results verified the known fact of poor efficiency for dielectric transducers. Although the B&K microphones were limited in the amount of applied voltage when used as a source, twice as much voltage applied to the dielectric transducers still yielded a much weaker signal. The difference of the ringing characteristic was considered less significant as a variation of 100 microseconds produces a 3.45 cm. spatial resolution change. Also an inherent discrepancy arose during the testing. The electret transducers appeared to produce results that decayed with repeated trials, indicating that the stability of the laboratory fabrication of the transducers was not on the same scale as B&K commercial production.

The conclusion was to abandon use of a dielectric transducer and revert to the previous findings--a bistatic combination of a 1" B&K source and 1/2" B&K receiver [Ref. 10].

C. SIGNAL PROCESSING

1. Source Signal

In order to obtain spectral analysis of a broad frequency range, the transmitted acoustic signal waveform must be composed of many frequencies. Ideally, an impulse would provide equal energy at all frequencies. However, a triangular waveform approximates an impulse on its positive going pulse and provides signals at all frequencies with harmonics of the fundamental predominant. The harmonic amplitudes decay at a rate of 6 dB per octave.

The Wavetek Model 175 Arbitrary Waveform Generator was used to generate the signal from stored waveforms or by programming any desired shape. A rise time of 500 nanoseconds of the triangular waveform allowed a close approximation to the infinite slope of an impulse. The waveform generator was triggered by the Interface Technology Model RS-648 timing simulator to provide a single pulse mode. This method presented the ability to separate the deisred scattered signal from other interference for each cycle of the output waveform.

The pulsed output was amplified by the Instruments, Inc., Model L-2 Power Amplifier to the maximum allowable voltage for the B&K microphones. For the 1" B&K, a total AC + DC voltage of 250 V is the limit. The best combination of polarizing voltage and AC driving voltage was 150 V and 100 V (peak to peak), respectively.

2. Received Signal

The received acoustic energy at the microphone was then amplified, bandpass filtered to eliminate low frequency noise and prevent aliasing, and amplified again to approach the maximum input limit of the A/D converter, ±10 volts. The amplifiers used were PAR Model 113 preamps due to their very low self-noise characteristics.

To separate the diffracted signal of interest from the stronger, unwanted signals of direct path travel, reflected travel from the surfaces, and diffraction from the edges; a sampling circuit was used to select a window coinciding at the time of the diffracted analog signal. The Interface Technology timing simulator accomplished the gating for the sampling frequency to 100 nanosecond accuracy.

The sampling circuit was built with IC devices, associated power supplies, and an oscillator. A General Radio Model 1312 coherent decade oscillator delivered the sampling frequency, since its stability characteristics provided the A/D converter with a constant frequency which allowed increased accuracy and repeatability of the data analysis. A schematic diagram of the circuit is illustrated in Figure 8. The circuit operates in the following manner. The decade oscillator porduces a constant frequency sine wave, which is then converted to the square wave form required by a A/D converter by a LM 710CN voltage comparator. The stable square wave output of the voltage comparator is combined

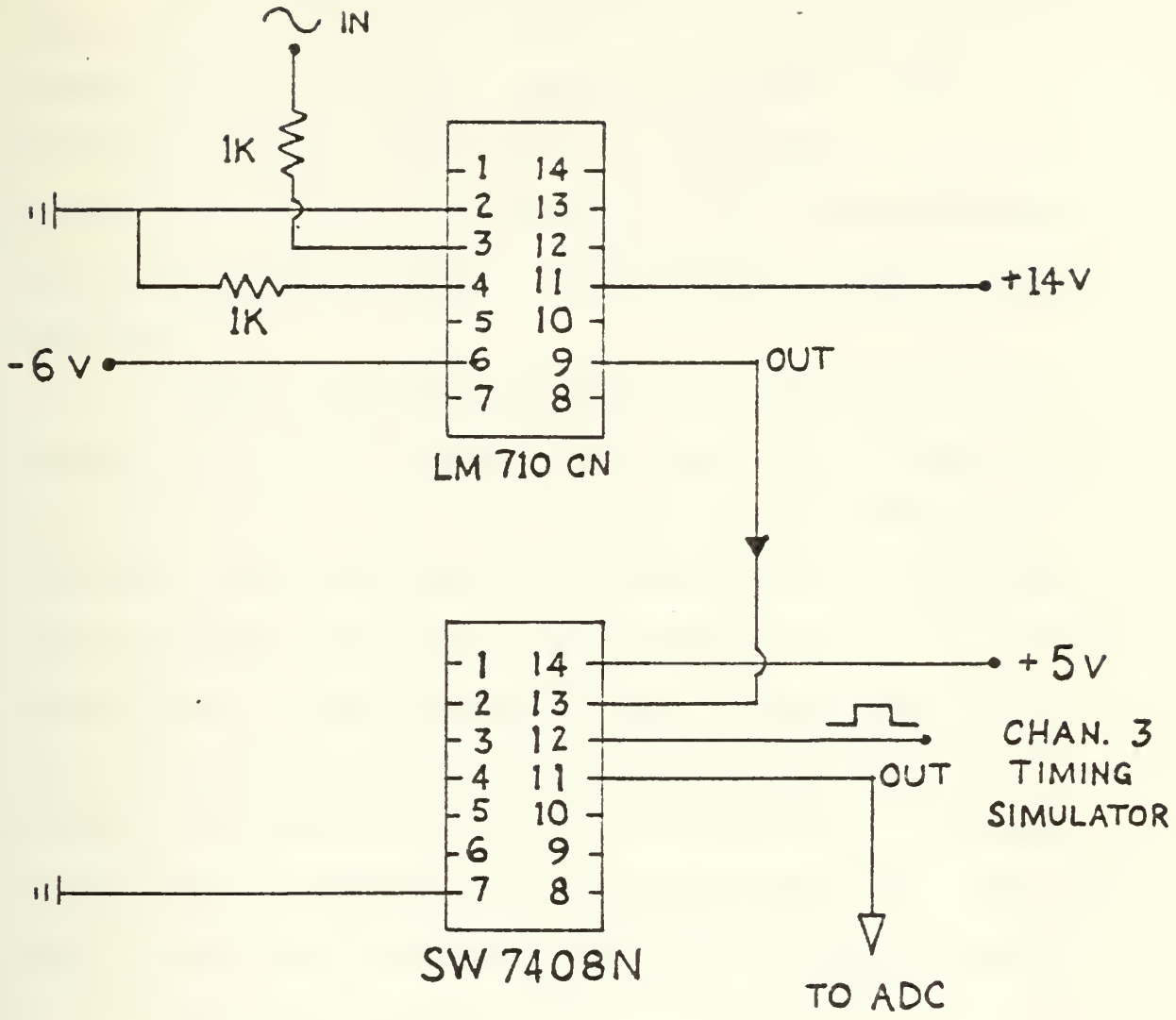

Figure 8. Sampling circuit

with the timing simulator pulse of duration for the desired aperture in a SW 7408N AND gate. The resulting output of the AND gate is a constant sampling frequency to the A/D converter only for the duration of the window. The input pulses to the A/D converter keyed the device to sample the analog signal being routed to the computer through the A/D converter.

Within a sampling aperture, the number of samples collected by the A/D converter was set to be a power of two; i.e., 64, 128, 256, etc., as required by the FOURONE FFT algorithm, which performed the transform for the frequency domain analysis. The sampling frequency was set at an integral multiple of the frequency of the transmitted signal. This relationship could be controlled by the decade oscillator and the Wavetek 175, thereby minimizing any truncation of the sampled waveform and eliminating sidelobes. The frequency resolution was determined by the following formula,

$$\frac{\text{sampling frequency}}{\text{number of samples}} = \text{frequency resolution}$$

However, the limiting value of frequency resolution was fixed by the duration of the sampling window.

The experiment was conducted with a 5 kHz transmitted signal and a 200 microsecond sampling window, which likewise set a 5 kHz frequency resolution in the output data. With this resolution determined, then a sampling frequency of 320 kHz would require 64 samples of data within the sampling

aperture. Following one cycle of signal transmission and received signal processing, a 20 millisecond delay was incorporated in the timing sequence to allow for complete decay of any reverberation before the next ping was triggered.

To improve the signal-to-noise ratio, an averaging routine within the computer software was performed on the digitized data. An ensemble of as many as 9,999 sampling windows could be selected for averaging prior to Fourier analysis. The signal-to-noise ratio could be increased by 10 log $\sqrt{N}$, where N is the number of averaging runs. Considering the trade-off of computer run time versus signal gain, 1,000 blocks of data were averaged to yield a 15 dB improvement. This averaged data was then used by the FFT algorithm, so that the computer output presented intensity by spectral distribution.

V. EXPERIMENTAL RESULTS AND ANALYSIS

A. BEAM PATTERN

Prior to determining the reradiated energy from the wedge or the rough surface, a beam pattern for the adjacent source-receiver combination was required to use as the reference pressure at a distance of one meter. The source-receiver combination (Fig. 9) was aligned to transmit at normal incidence toward a rigid, smooth plate. The source-receiver set-up was then rotated through $\pm 90^{\circ}$, so that the received signal described the beam pattern for the source-receiver combination. This procedure was performed for two arrangements that are called the symmetrical and asymmetrical cases. In the symmetrical case, the source and receiver are aligned relative to each other vertically (parallel) with respect to the axis of rotation, and in the asymmetrical case, they are horizontal (perpendicular) to the axis. As the combination is rotated in azimuth, both the source and receiver are the same distance from the rigid reflector for the symmetrical situation. However, in the asymmetrical arrangement, either the source or receiver is closer to the rigid plate than the other depending upon the direction of rotation.

The resulting beam patterns for the two situations are presented in Figures 10 through 14 for various frequencies.

Interestingly, the two patterns are quite similar regardless of the relative position of the source and receiver to

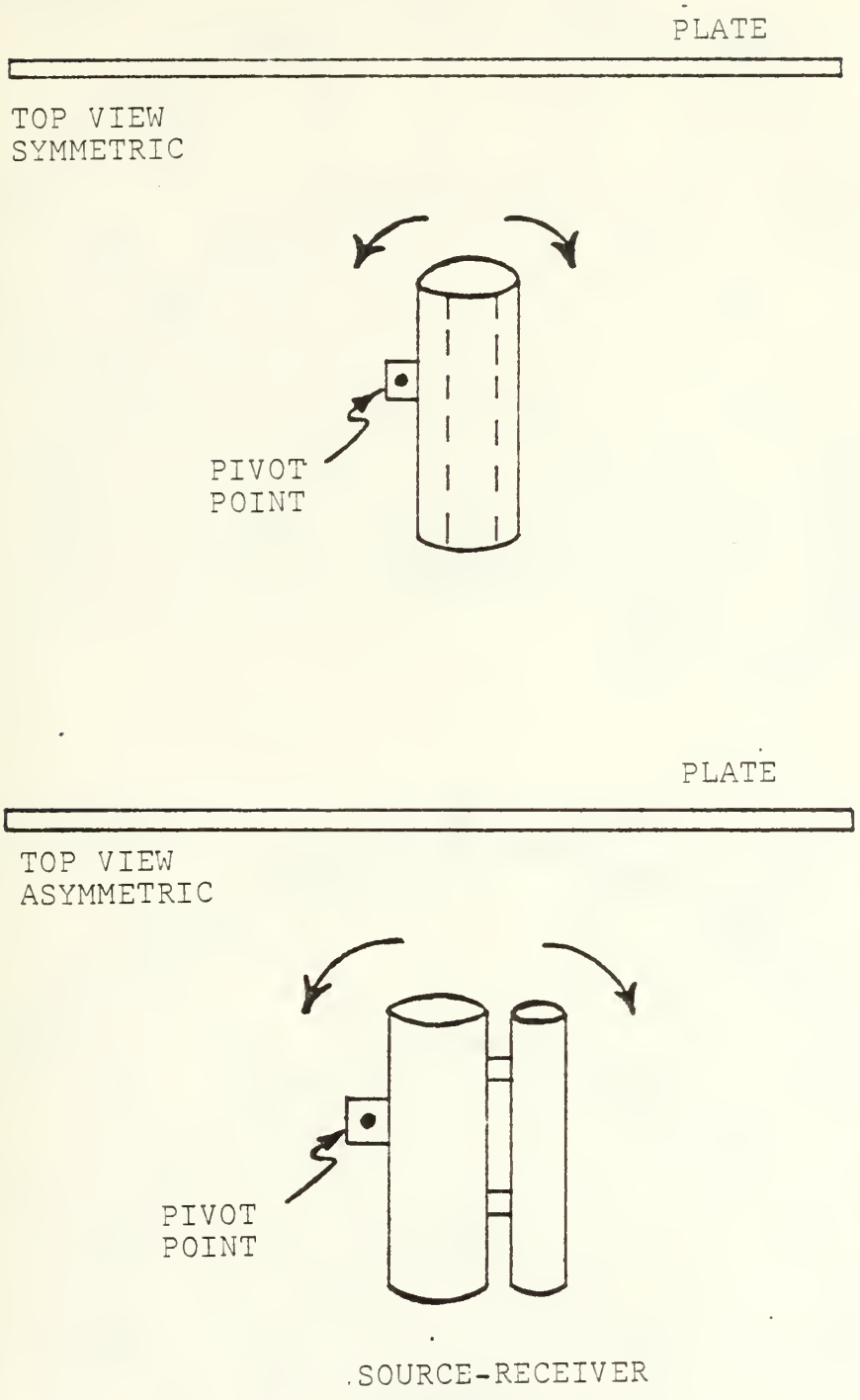

Figure 9. Beam pattern source-receiver arrangement

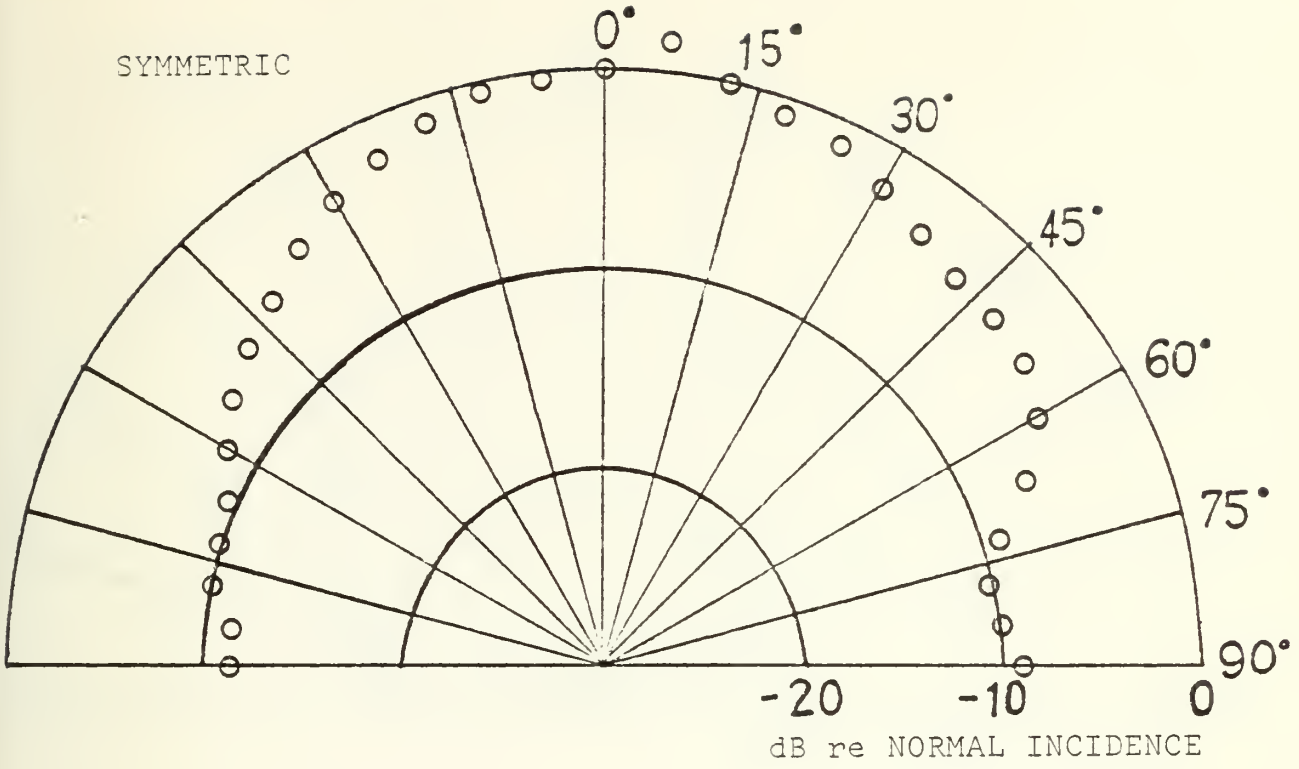

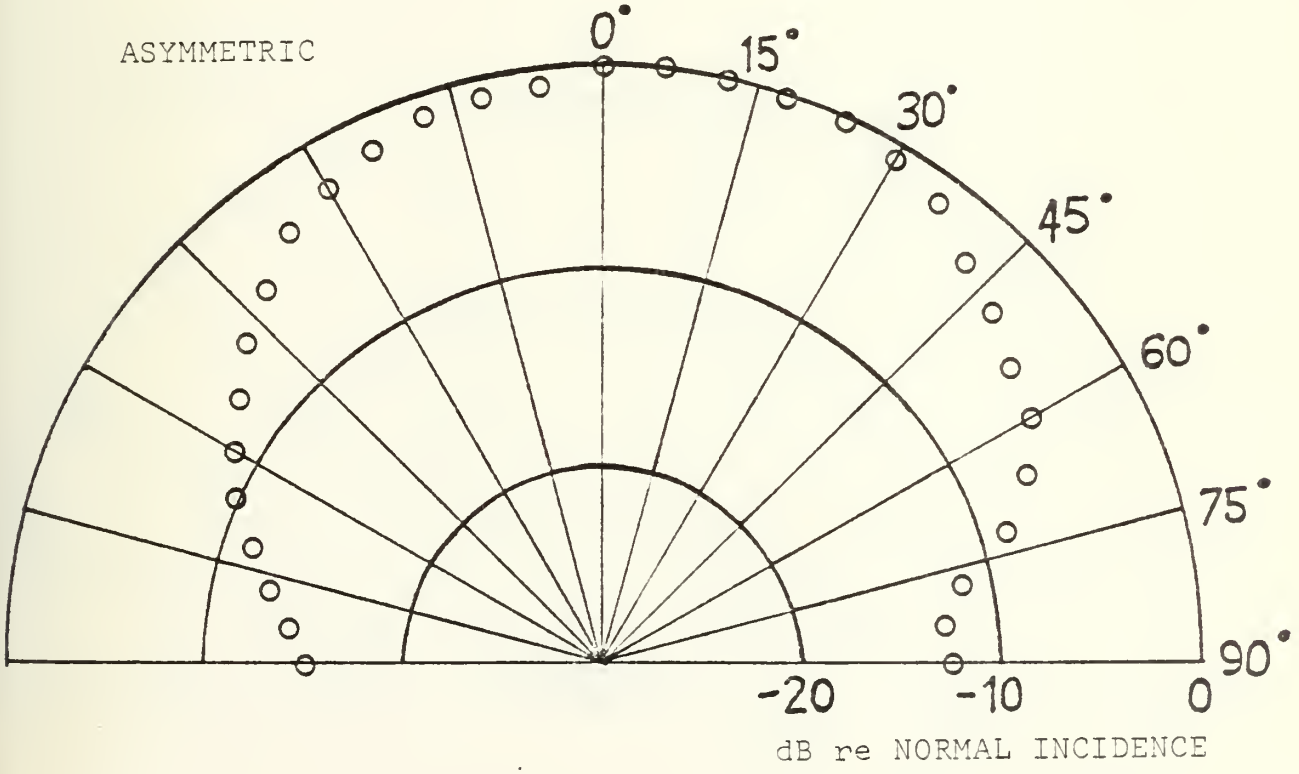

Figure 10. Beam pattern for 10 kHz

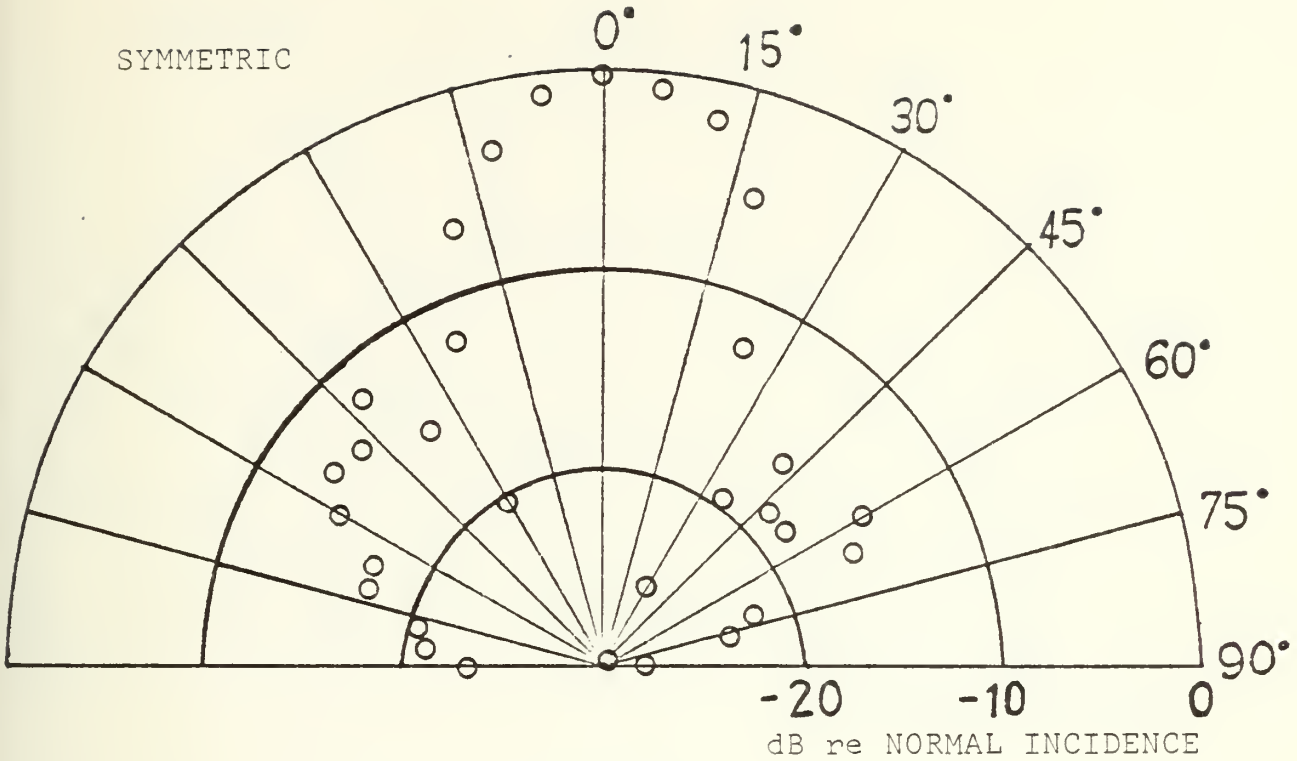

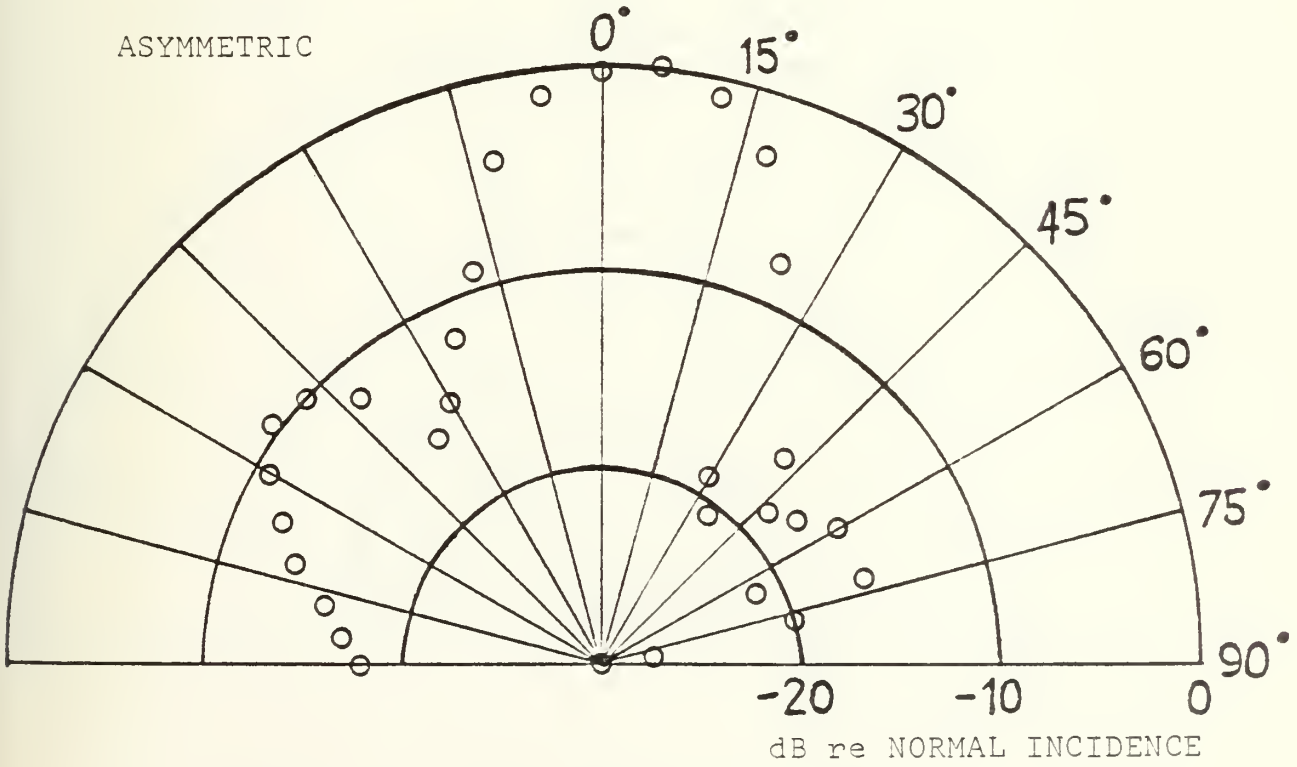

Figure 11. Beam pattern for 30 kHz

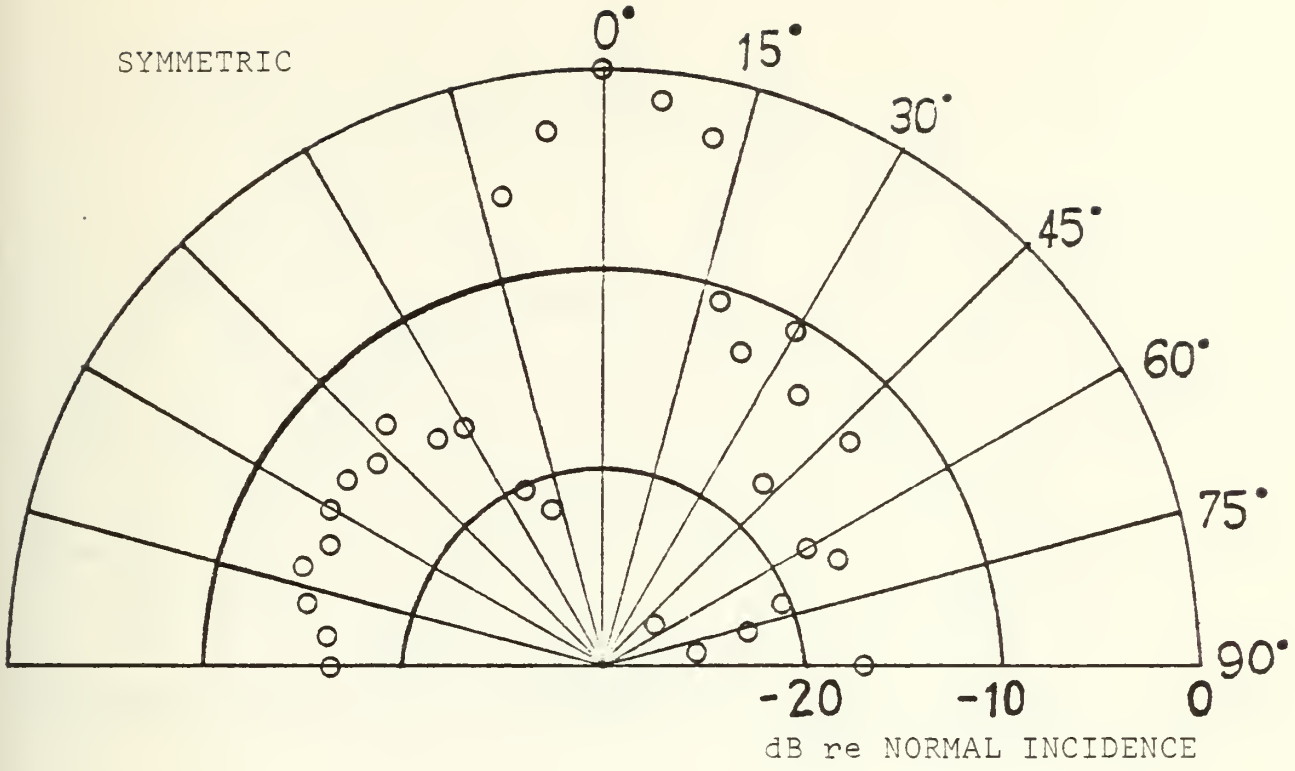

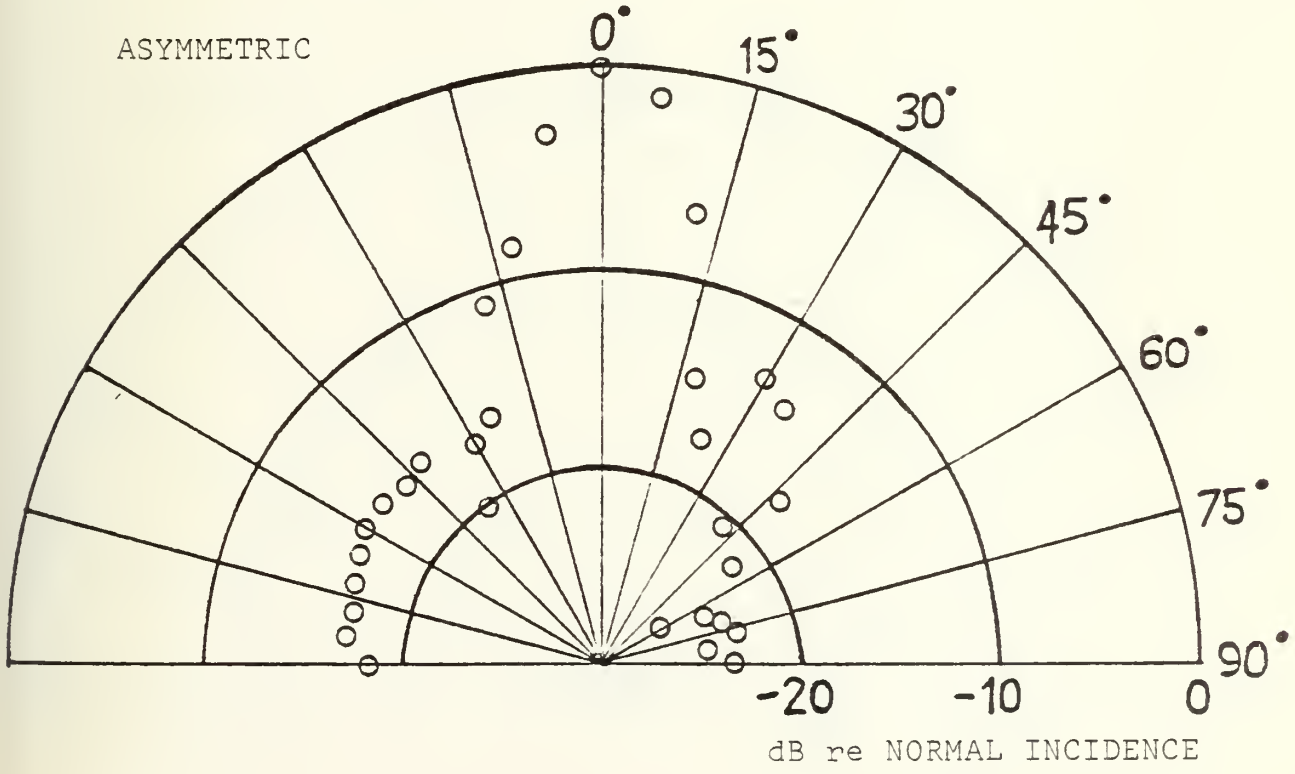

Figure 12. Beam pattern for 50 kHz

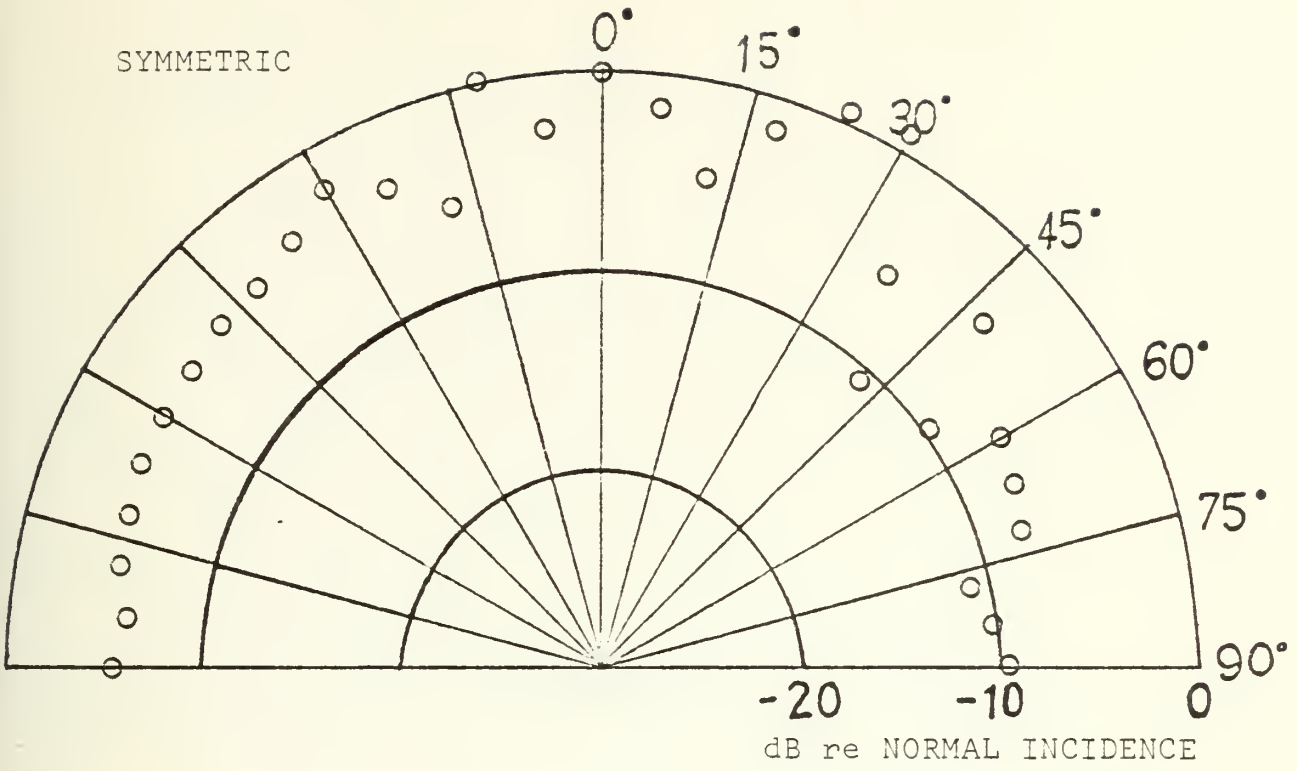

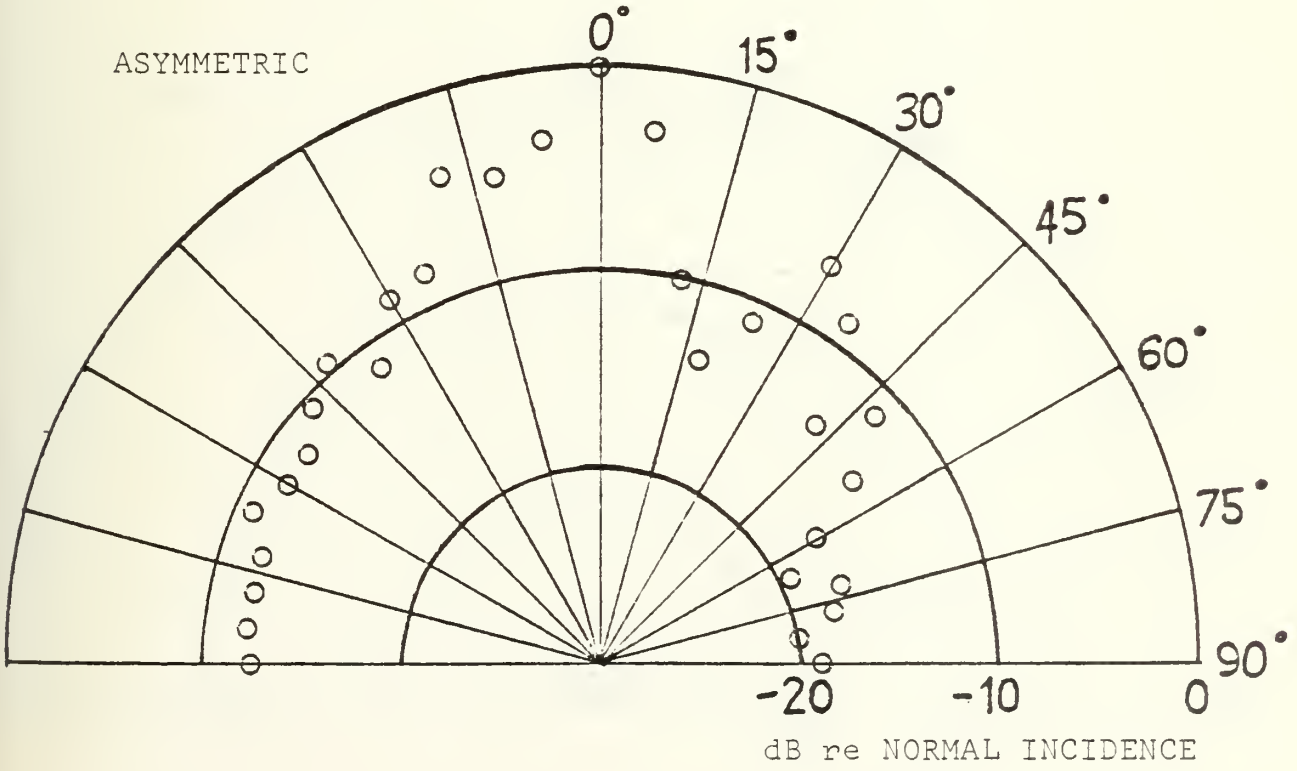

Figure 13. Beam pattern for 70 kHz

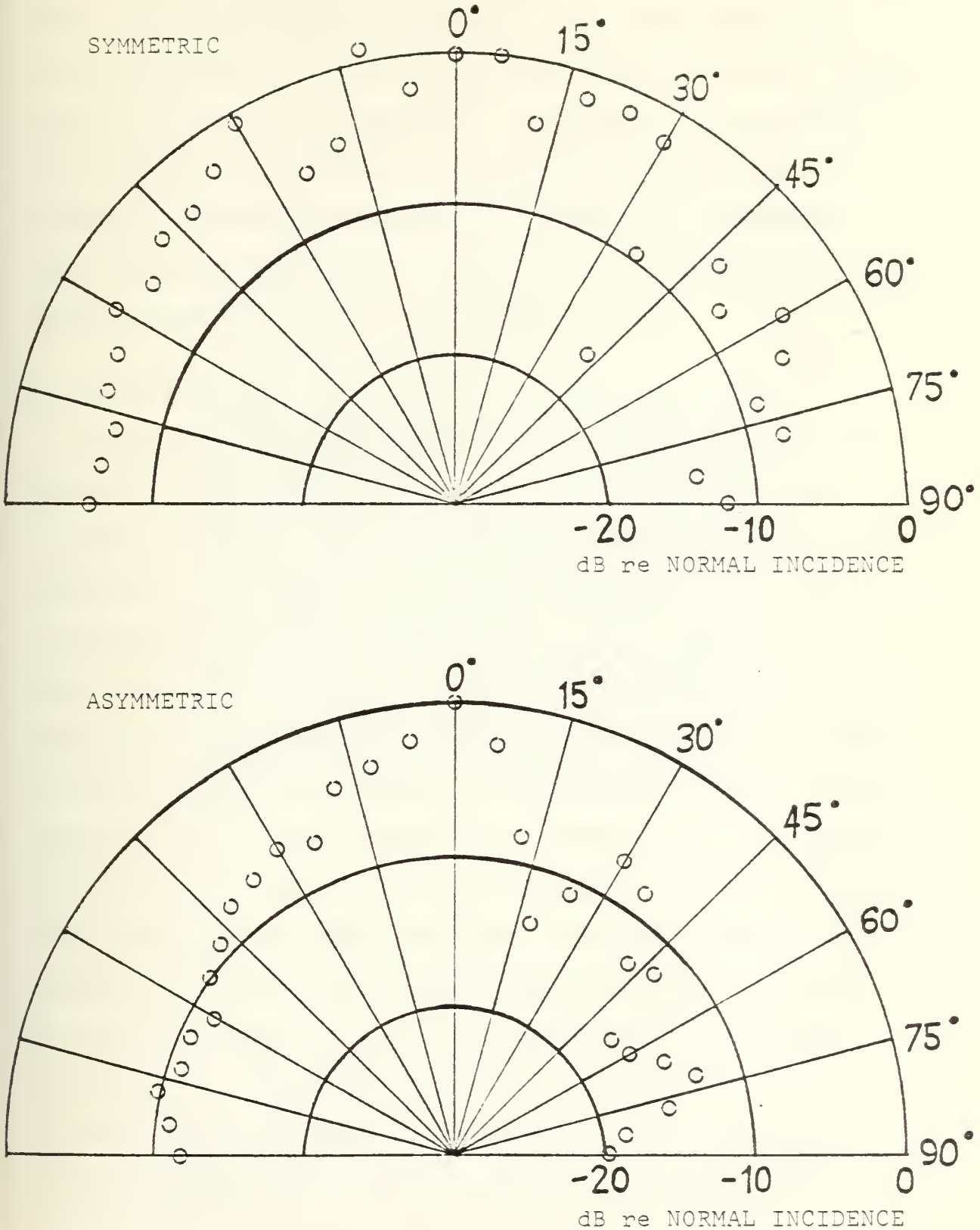

Figure 14. Beam pattern for 100 kHz

the reflecting plate. This can be accounted for by the fact that the 200 microsecond aperture of the received signal processing is long enough to include the diffraction results from the adjacent microphone in either spatial arrangement. The dissimilarity between the right and left halves of the pattern is likewise consistent throughout the frequency range and results from the diffraction effects of the source-receiver combination and the mounting set-up.

B. SMOOTH WEDGE

To measure the backscatter from the crest of the wedge, the source-receiver acoustic axis was aimed at the crest (z-axis of wedge). The position of the source-receiver relative to the wedge was varied to compare to the theory for the respective geometry. The position was defined by the slant range from the crest to the source-receiver and by the angle between the acoustic axis and the wedge. The geometry of the experiment was limited by the interference of unwanted signals when the crest backscatter could not be individually gated from the other returns. Figure 15 shows an oscilloscope trace of the received signal with the three returns separated in time. The initial, large amplitude (clipped in picture) signal is the direct wave which is received immediately. The reflected signal due to normal incidence of the side lobe appears at approximately 820 microseconds, and the backscattered return from the crest arrives at

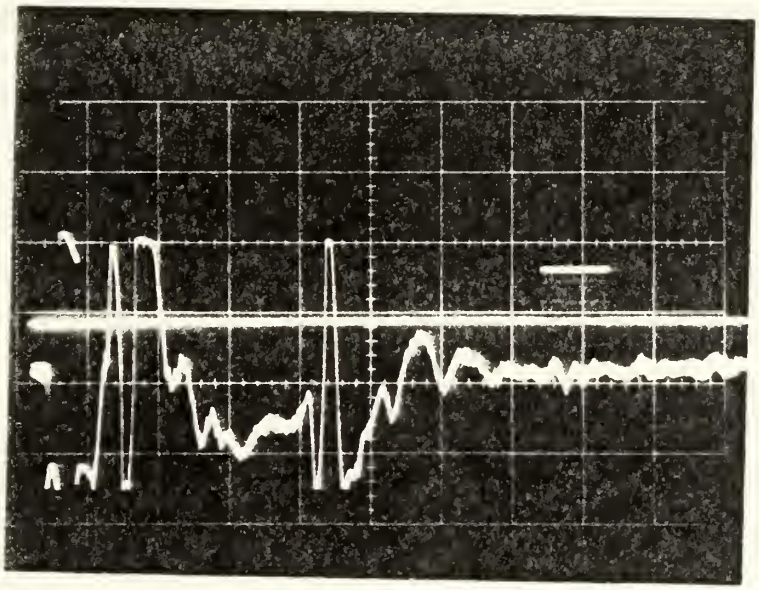

Figure 15. Typical oscilloscope trace of direct, reflected, and diffracted signals from smooth wedge

approximately 1.5 milliseconds. The square pulse above the received signal shows the sampling aperture for gating the return to be analyzed.

The geometry of Figure 4 and the picture in Figure 15 show how the source-receiver position limitations are imposed. If the source-receiver is too close to the crest, the backscatter will be masked by the stronger direct and reflected returns. If the range is kept constant, but the angle is increased, the reflected signal is delayed in time and overshadows the backscatter again. If the range is increased to more than half the length of the side of the wedge, diffraction from the back edge interferes with the diffraction of interest from the crest. To determine the position limitations numerically, data collection was conducted at angles of 0°, 10°, 20°, 30° at both 25 cm. and 30 cm. Figures 16 through 23 show the normalized, backscattered intensity plotted versus frequency. It is noted that the backscatter for a wedge can be defined by the quantity of backscattered signal strength (BSS),

$$BSS_W = 10 \log\left[\frac{I_{BS}}{I_0} \frac{r^2}{r_0} \frac{r}{\lambda}\right]$$

where I_0 is the intensity at one meter. However, since it is the intensity ratio which is calculated in the signal processing, this is the quantity used in the comparison with theory. In theory, I_{BS} is inversely proportional to frequency for a wedge at high frequencies (Ref. 7).

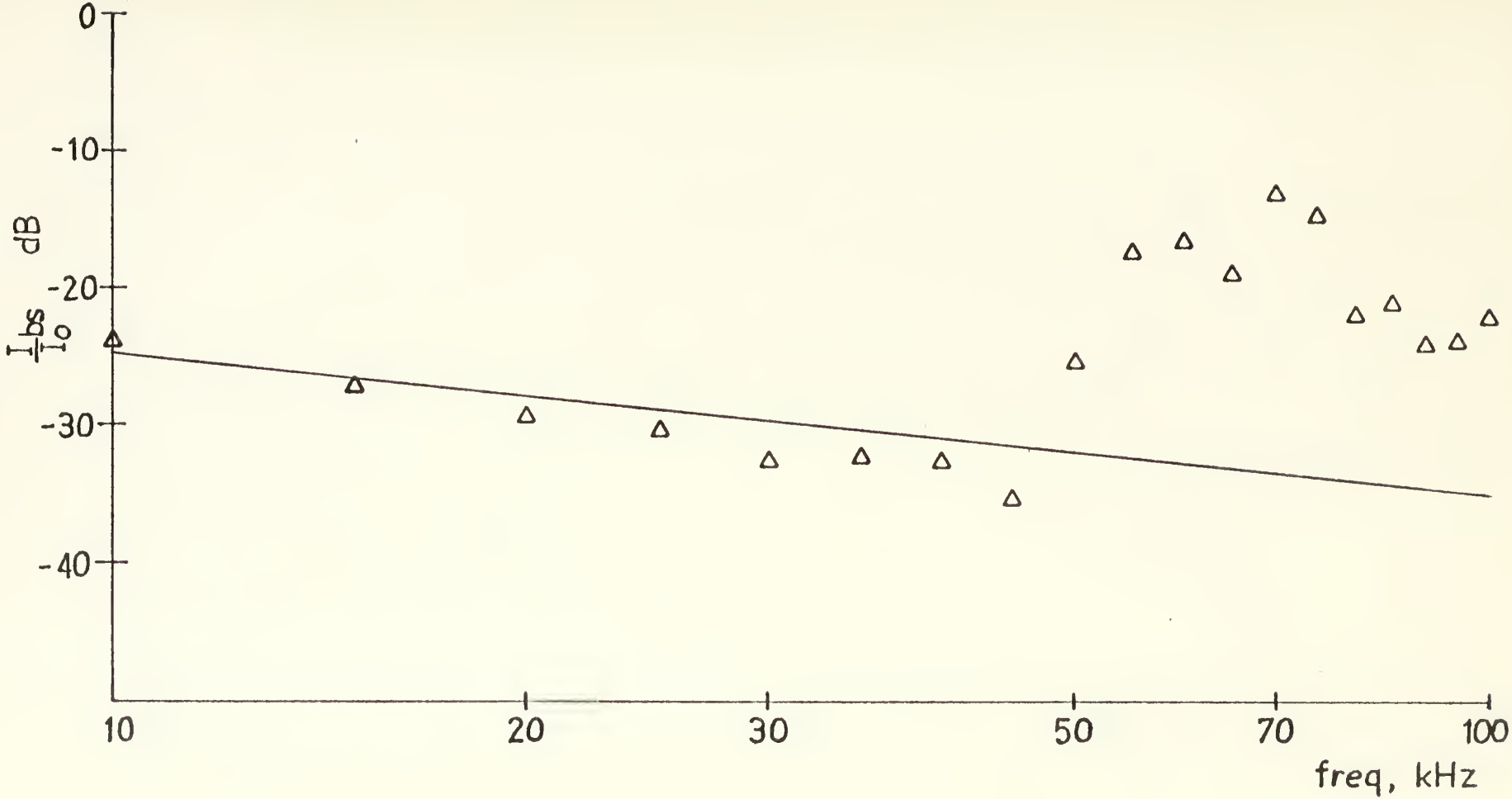

Figure 16. Smooth wedge backscatter, $r = r_0 = 25$ cm, $\theta = \theta_0 = 0^\circ$; experimental data ($\Delta$), theory ($\underline{=}$).

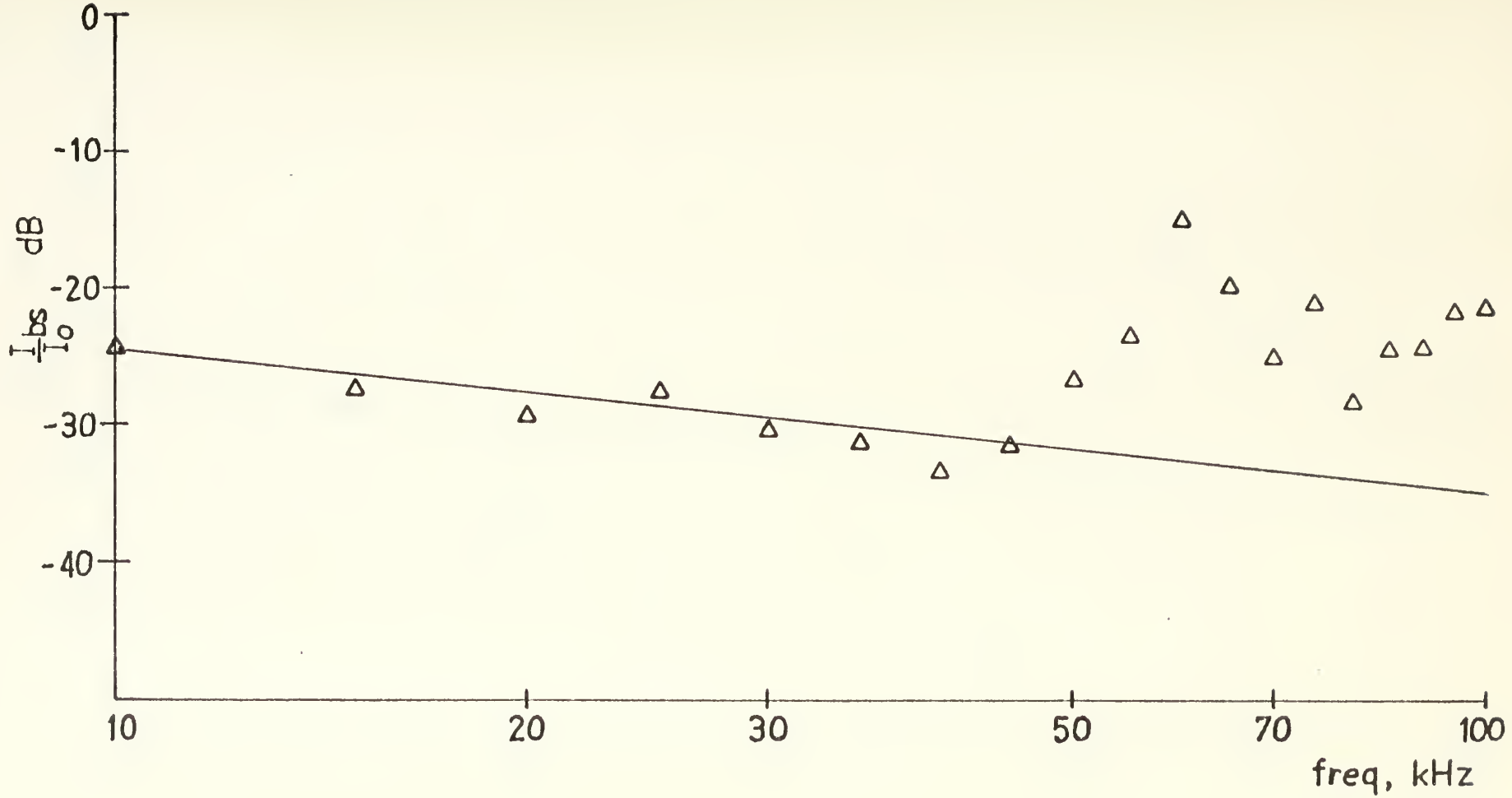

Figure 17. Smooth wedge backscatter, $r = r_0 = 25$ cm, $\theta = \theta_0 = 10^\circ$; experimental data ($\Delta$), theory ($\frac{0}{-}$).

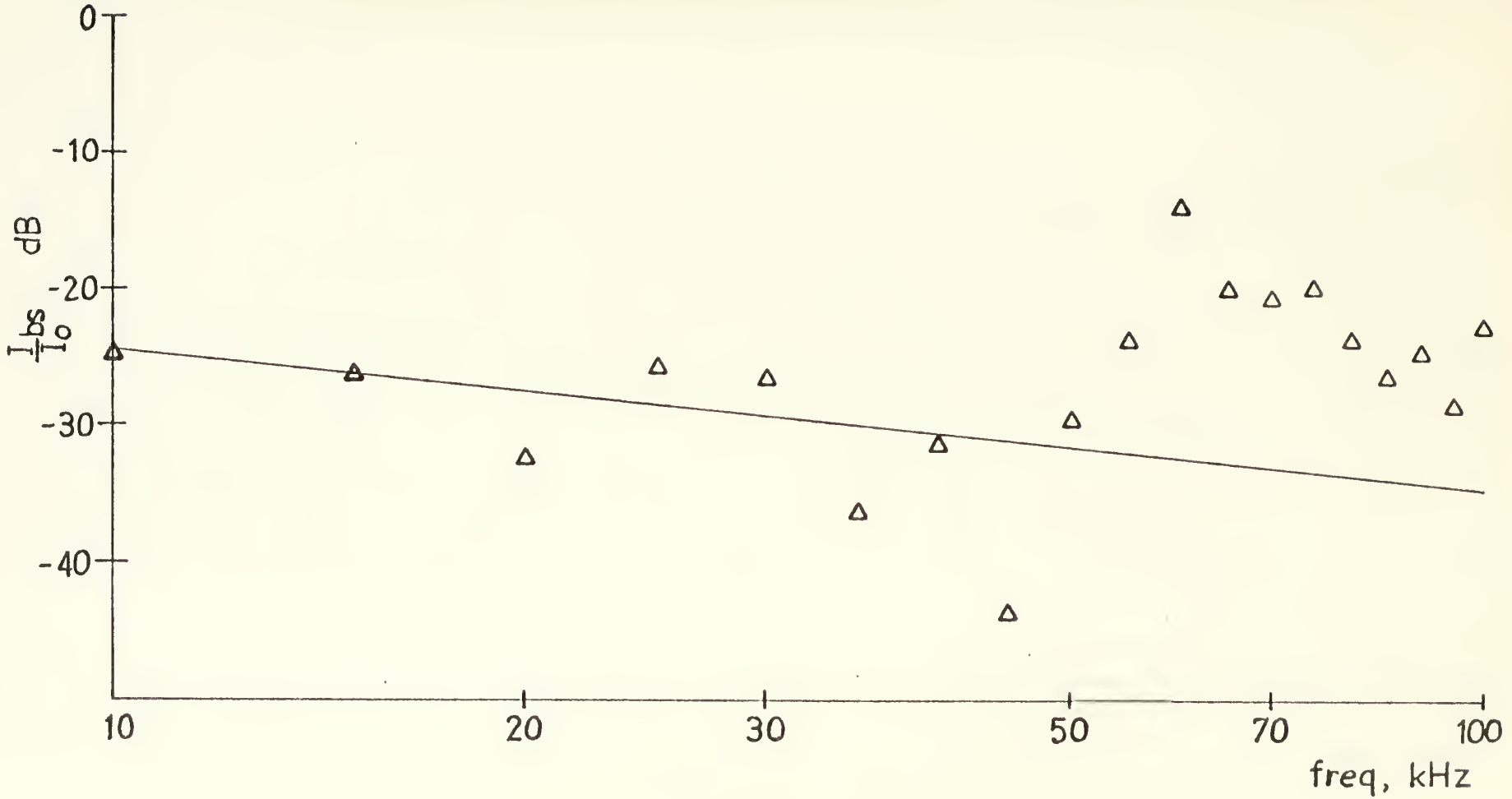

Figure 18. Smooth wedge backscatter, $r = r_0 = 25$ cm, $\theta = \theta_0 = 20°$; experimental data (Δ), theory (—).

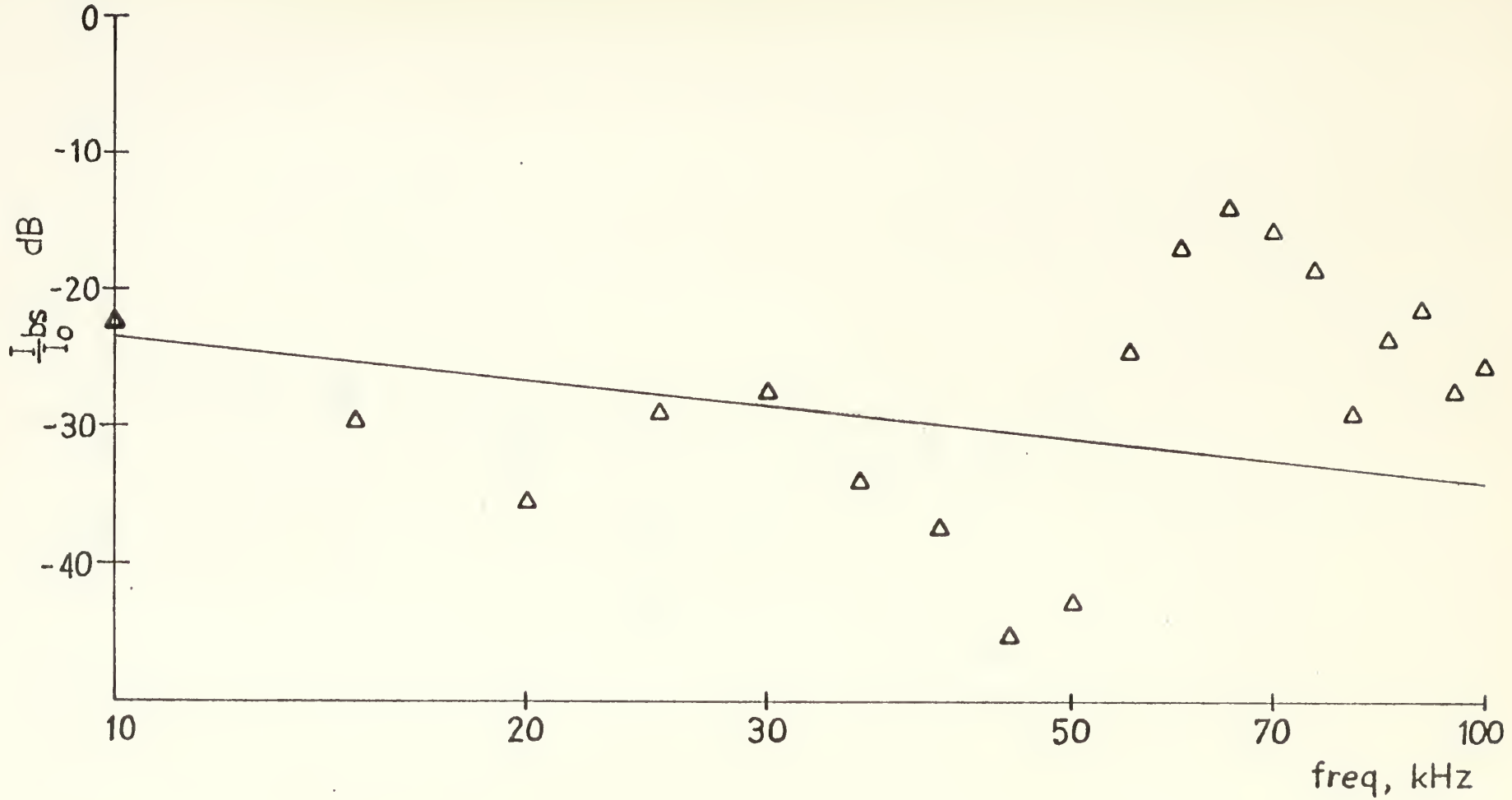

Figure 19. Smooth wedge backscatter, $r = r_0 = 25$ cm, $\theta = \theta_0 = 30°$; experimental data (Δ), theory (-).

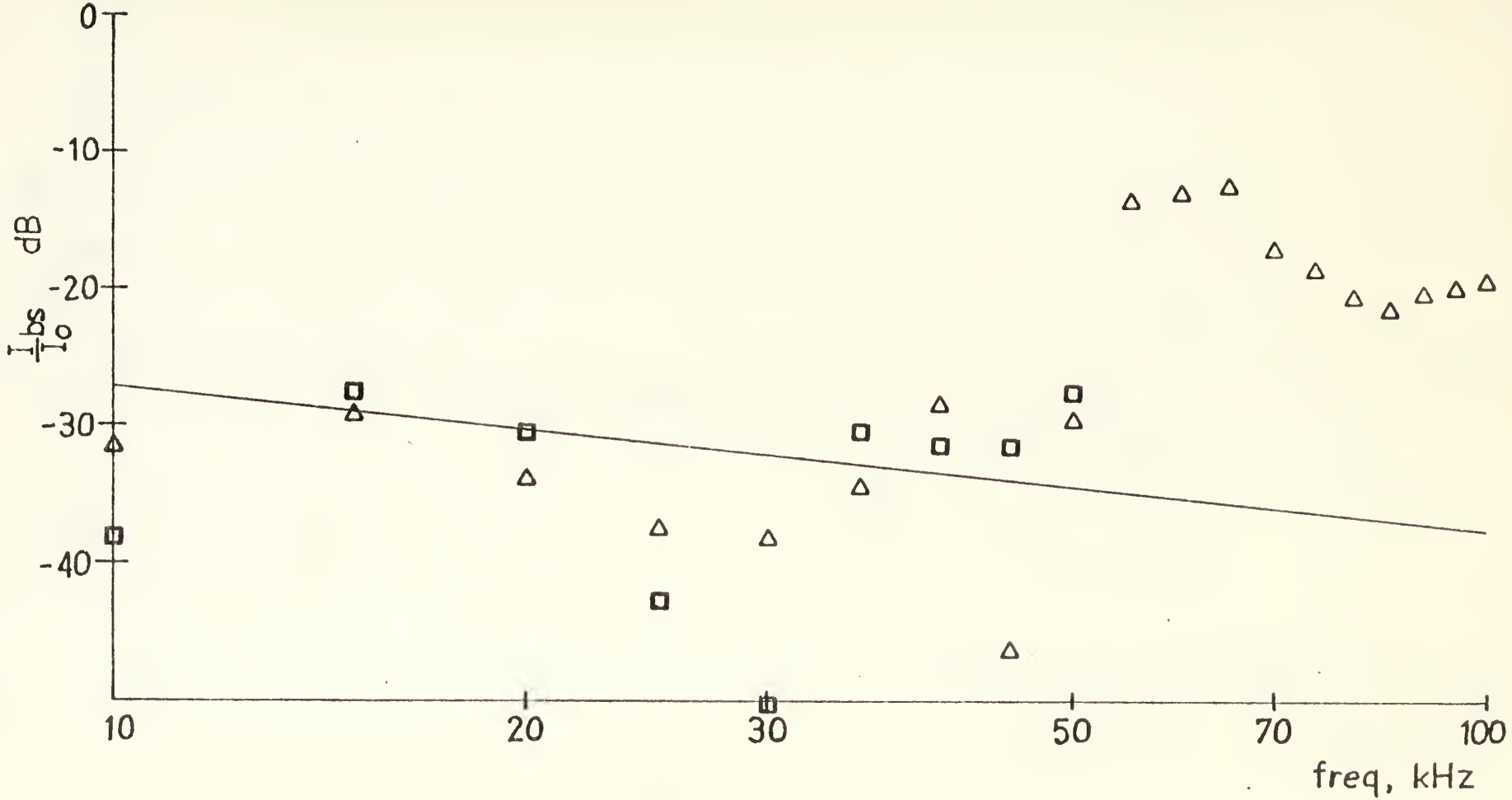

Figure 20. Smooth wedge backscatter, $r = r_0 = 30$ cm, $\theta = \theta_0 = 0°$; experimental data (Δ), data for wedge with extension (□), theory (-).

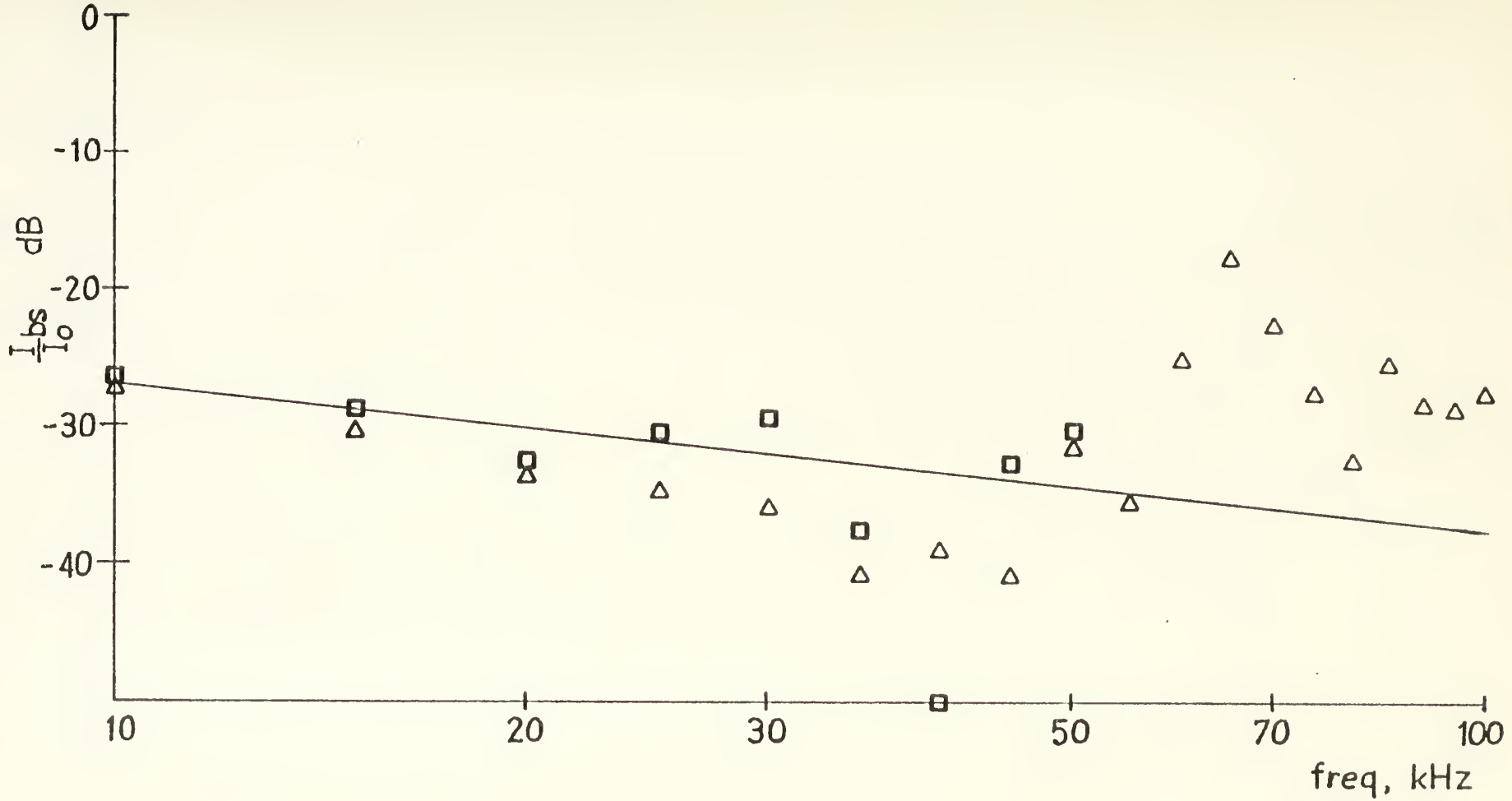

Figure 21. Smooth wedge backscatter, $r = r_0 = 30$ cm, $\theta = \theta_0 = 10^\circ$; experimental data (Δ), data for wedge with extension (□), theory (-).

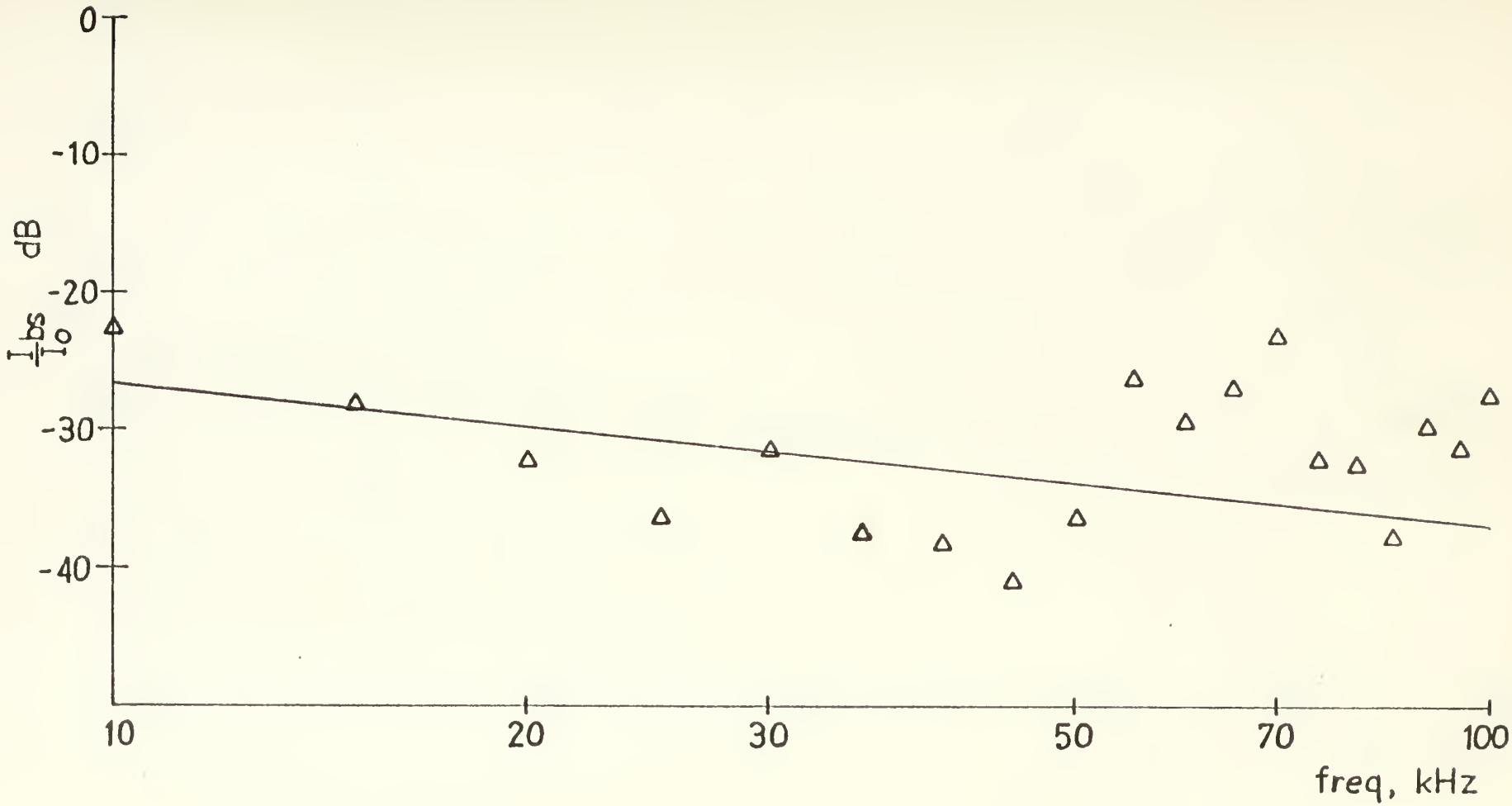

Figure 22. Smooth wedge backscatter, $r = r_0 = 30$ cm, $\theta = \theta_0 = 20°$; experimental data (Δ), theory (-).

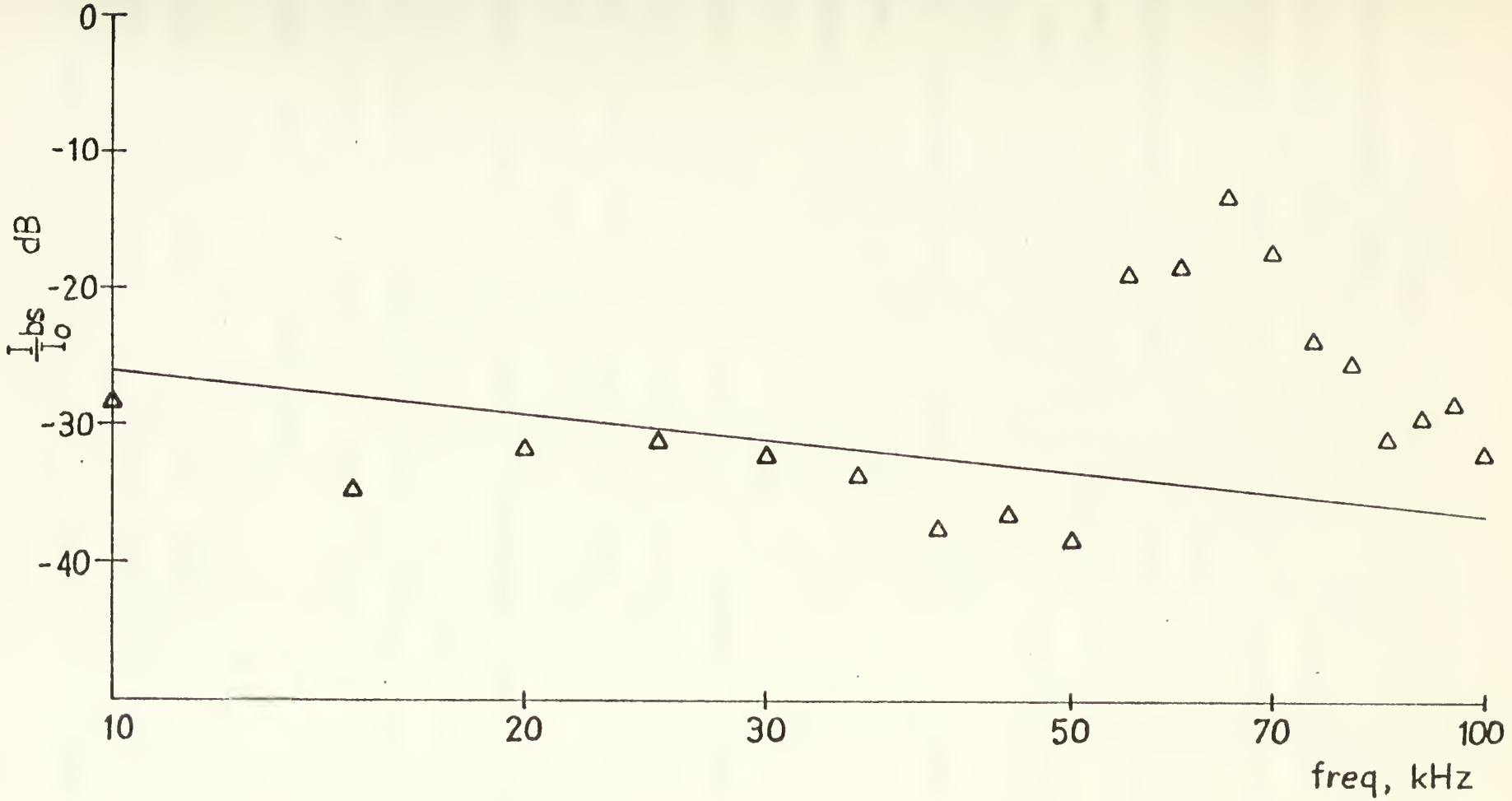

Figure 23. Smooth wedge backscatter, $r = r_0 = 30$ cm, $\theta = \theta_0 = 30°$; experimental data (Δ), theory ($\frac{0}{-}$).

The received signals were time averaged 1000 times in a 200 microsecond sampling aperture to obtain a signal-to-noise ratio (S/N) ranging from 5 to 30 dB throughout the frequency spectrum; Figure 24 shows the relative S/N for the three surfaces. The noise was measured with both source and microphone on but with a data window corresponding to a region of nonscatter in the anechoic chamber.

The results of Figs. 16-23 indicate a major consistent deviation from theory for the frequency range above 50 kHz. This can be explained by reverting to the beam pattern diagrams. At the ranges of the experiment, the 200 microsecond processing window for the returned signal subtends a half-angle of 28°. This angle of insonified area should be within the main lobe of the source-receiver pattern to insure symmetry and approximate a point source. The plot for 50 kHz approaches this critical condition where the rapid fall-off from the main lobe is within the angle of collected data. However, the polar plots for the higher frequencies show increasingly asymmetrical patterns near the acoustic axis and lack of a well-defined lobe pattern expected at those frequencies. This non-uniformity and deviation from a point source lobe renders the data above 50 kHz unreliable.

At the 25 cm. range, the data up to 50 kHz shows close agreement with theory for the low angles of 0° and 10°. However, as the angle is increased, the interference from the reflected signal causes an increasing oscillation of the

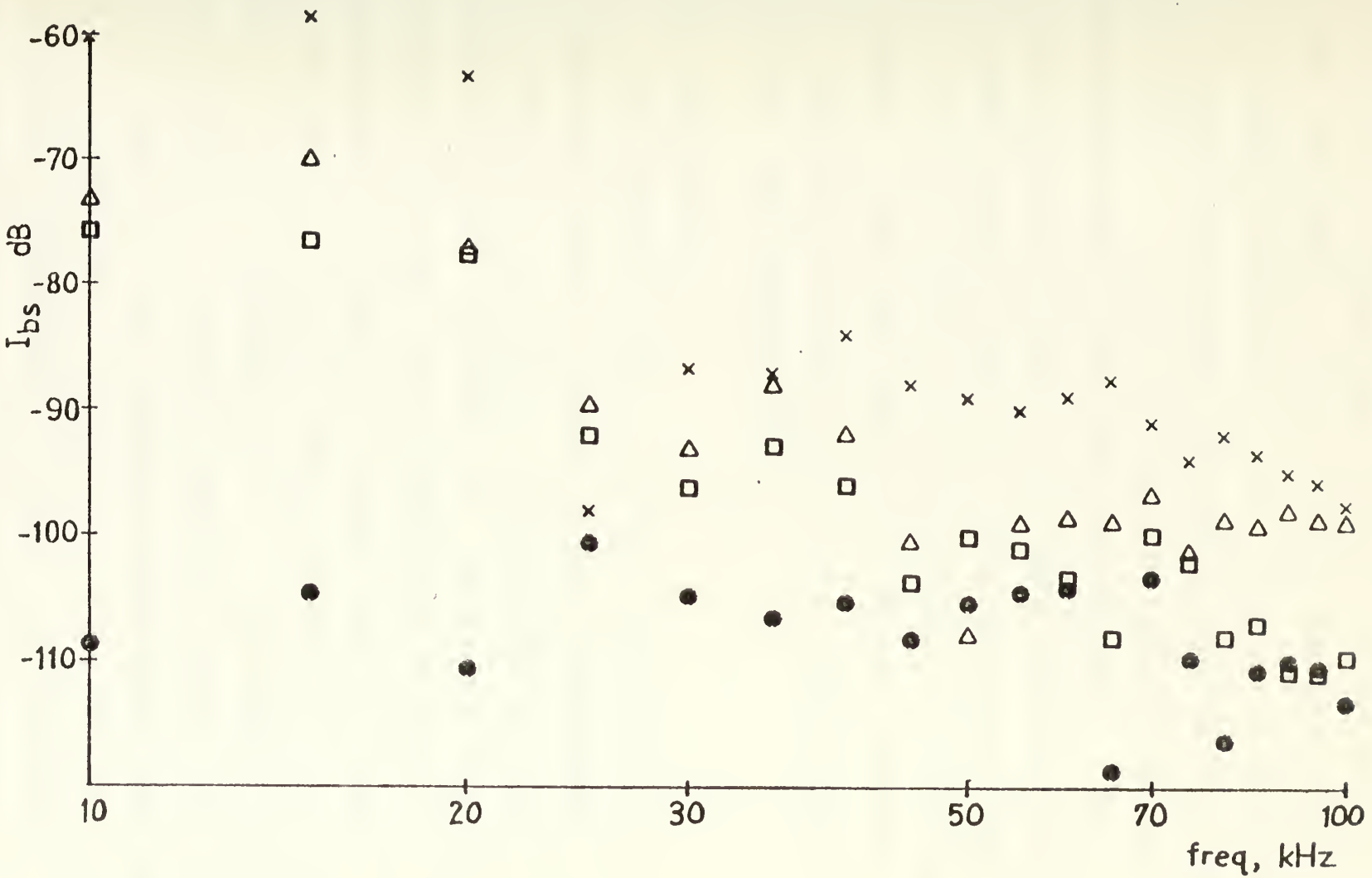

Figure 24. Comparison of wedge backscatter for various surfaces, $r = r_0 = 25$ cm, $\theta = \theta_0 = 0°$; smooth wedge (□), wedge with lead shot surface (△), wedge with gravel surface (x), noise level (●).

data about the theoretical curve. The plots for the 30 cm. range show similar results, although the lower angles do not compare as well as at 25 cm. This can be attributed to the concurrent diffraction signal from the back edge of the plate. A plywood extension was added to the plate to see if the data at 30 cm. could be improved. The extension, with resulting reduction of back edge diffraction, improved the data slightly, except for one or two points, which may be due to the impedance mismatch between the plywood and aluminum. From these results, the geometry was restricted to frequencies no greater than 50 kHz, grazing angles of 0° and 10°, and a range of 25 cm.

C. ROUGH SURFACE

The backscatter from a randomly rough surface due to a transmitted signal at normal incidence was measured in order to compare to experimental and theoretical scattering results reported by Clay and Medwin [2]. Previous studies deal with surfaces with small slope roughnesses and conclude that the backscattered intensity will be the sum of a coherent component and an incoherent component with the coherent dominant at $g << 1$ and incoherent at $g >> 1$. The measured statistic of rms height, σ, should be comparable to the value calculated from acoustical normal incidence backscatter in the range of $g < 1$ as described in Section III.B. The lead shot surface presented a backscattered intensity (not normalized) at normal incidence that was almost identical in shape and deviated

less than 5 dB from the backscattered intensity from a smooth surface (Figure 25). The fact that for most frequencies the return from the wedge covered with lead shot yielded a slightly greater signal than from the smooth surface may have been the result of incoherent contribution of backscatter from multiple large slope off-axis scatterers. The similarity of these curves and the small dimensions of the lead shot compared to the sound wavelength led to the tentative conclusion that this surface appeared nearly "acoustically smooth" for the frequency range of interest. The term "acoustically smooth" is used in the classical sense, $g << 1$.

The experiment now shifted to data collection from surfaces coated with gravel to present a greater degree of roughness.

Two methods were used to derive the statistical parameters of the surface. In the acoustical technique, the normal incidence mean-squared backscattered pressure (normalized to squared pressure received from smooth surface at the same range) was plotted as in Figure 26. The backscattered pressure was measured at four regions of the rough surface, to obtain the mean squared pressure. Comparison of the curve with theory (eqs. 27, 29) was used to extract the rms height and correlation length. Alternatively, a small sample plate of gravel roughness was constructed. The heights in a 5 cm. square area were sampled every 0.1 mm. to provide a 2500 point data base for calculating the same statistical parameters.

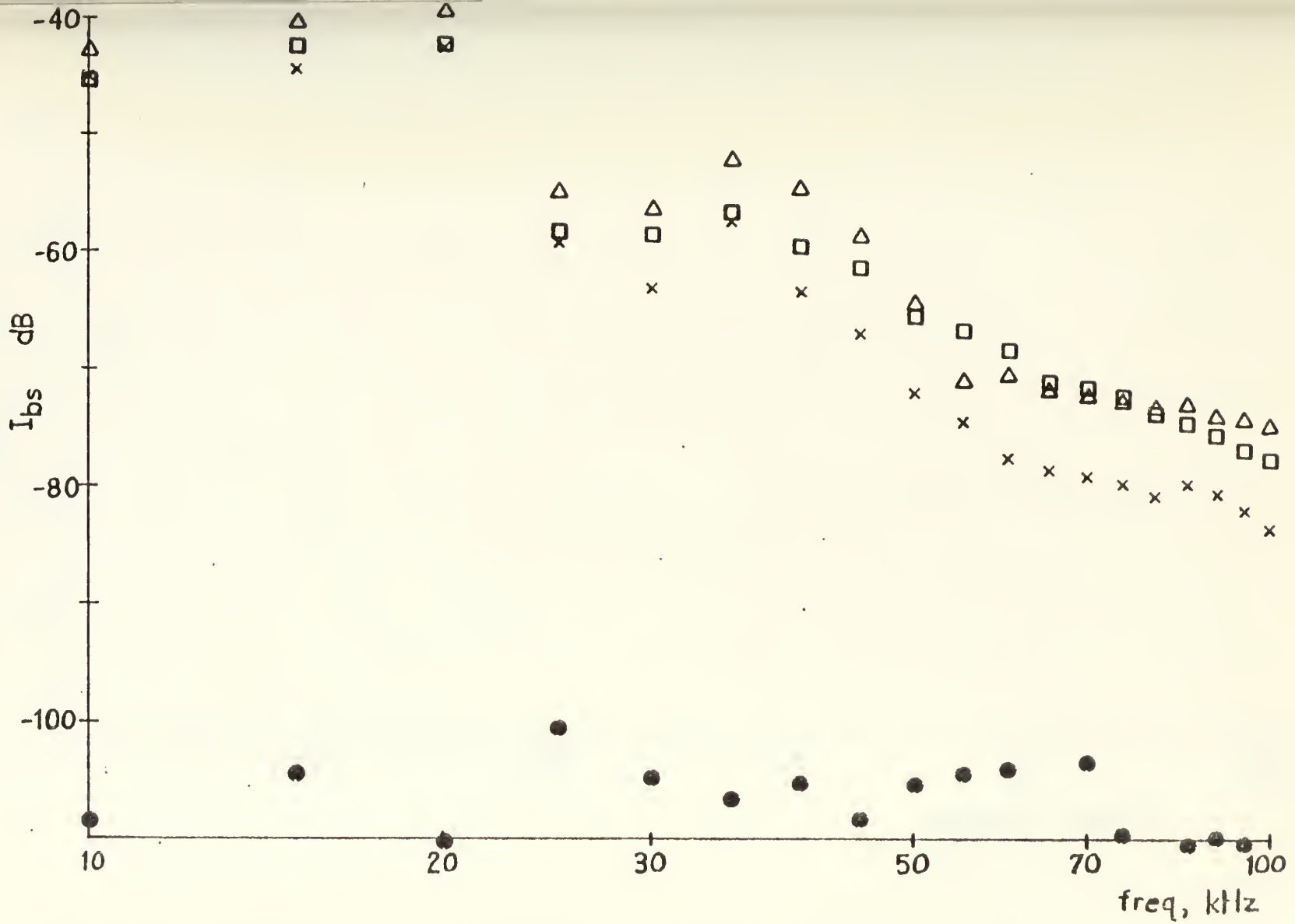

Figure 25. Comparison of backscatter for various surfaces at normal incidence, $r = r_0 = 25$ cm.; smooth plane surface (□), plane surface with lead shot (Δ), plane surface with gravel (x), noise level (●).

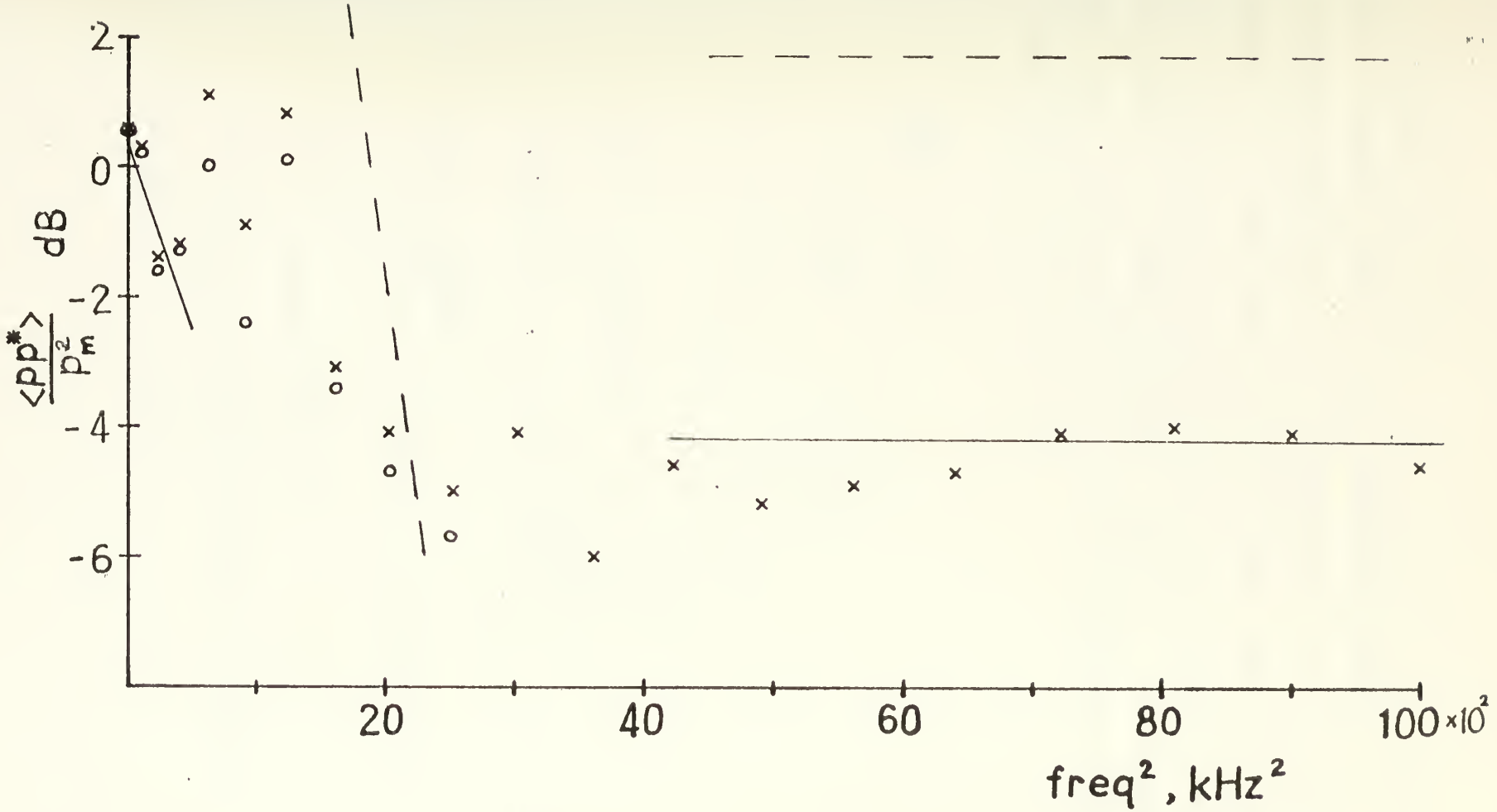

Figure 26. Mean-squared pressure from gravel surface at normal incidence, $r = r_0 = 25$ cm.; coherent component, $\langle p \rangle^2/p_m^2$, (o), slope and asymptote from acoustical data (solid line), slope and asymptote from surface statistics (dashed line).

Theoretically, for $g << 1$, the log of the relative intensity is proportional to the roughness parameter, g. The roughness parameter (g) is related (see eq. 22) to the rms height (σ), which can now be obtained. The latter parameter and the asymptotic value that the curve approaches enable calculation of the correlation length (L). The backscatter data were plotted against f^2 and estimates from data in Figure 26 were calculated as follows,

$$\frac{I_{BS}}{I_0} = e^{-g}$$

$$10 \log \frac{I_{BS}}{I_0} = -10\, g \log e$$

$$g = k^2\sigma^2 (\cos\theta_1 + \cos\theta_2)^2$$

for 90° backscatter, $g = 4k^2\sigma^2$

$$10 \log \frac{I_{BS}}{I_0} = -4.343 \left(\frac{16\pi^2 f^2}{c^2}\right)\sigma^2 \qquad c = 345 \text{ m/s}$$

$$\frac{\Delta\left[10 \log \frac{I_{BS}}{I_0}\right]}{\Delta[f^2]} = \text{slope} = (-5.762 \times 10^{-7})\sigma^2$$

$$\sigma^2 = 6.94 \times 10^{-3} \text{ cm}^2$$

$$\sigma_{acoustical} = 8.30 \times 10^{-2} \text{ cm} = 0.83 \text{ mm}$$

$$\sigma_{msrmt} = 2.23 \text{ mm}$$

and

$$\text{ASYMPTOTE}\Big|_{g>>1} = \frac{AL^2}{2\sigma^2 r^2}$$

$$L = \left[\frac{(\text{ASYMPTOTE})\,2\sigma^2 r^2}{A}\right]^{1/2}$$

ASYMPTOTE = 0.38

$\sigma = 8.3 \times 10^{-2}$ cm

r = 25 cm

A = 579. cm^2 from window opening

$L_{Acoustical} = 7.73 \times 10^{-2}$ cm = 0.77 mm using $\sigma_{acoust.}$

$L_{Acoustical} = 2.0$ mm using σ_{Msrmt}

$L_{Msrmt} = 4.0$ mm.

The statistical measurements performed by Jordan [11] on the sample gravel plate yielded values of σ = 2.23 mm. and L = 4.0 mm.

Although the shape of the plotted data seems promising, the differences in the two statistical parmaeters are evident by the plot. The slope shown leads to σ = 0.83 mm. vice surface measured σ = 2.23 mm. Similarly, the acoustically determined correlation length is 0.77 mm. vice the surface measurements 4.0 mm. The large discrepancies between measured and acoustically determined statistical parameters can be

explained by the inappropriate theoretical description of the rough surface and the inability to use a large number of scattering surfaces for the experimental determination of $\langle p \rangle^2 / p_m^2$. The experiment used gravel that presented a jagged rough surface with steep slopes and cusp-like features, whereas the acoustic scattering theory from which σ and L were calculated assume a gently changing slope for the rough surface.

The experiment next proceeded to identify the effects of both a wedge and the rough surface on the backscattered sound. The backscattered signal strength (BSS_s) for the rough surface alone is expressed by the equation for incoherent point scatters,

$$BSS_s = 10 \log\left[\frac{I_{BS}}{I_0} \frac{R^4}{R_0^2 A}\right] .$$

This definition of BSS assumes that the intensity diverges as R^{-2} from source to scatterer, and R^{-2} from point scatterer to receiver for a net divergence of R^{-4}. The point scattering assumption was verified for frequencies above 50 kHz at normal incidence backscatter. This supports the assumption of point scattering at all lower frequencies, and at grazing as well as normal incidence. The total signal returned from a rough surface and wedge is the sum of these scattering effects,

$$BSS = 10 \log\left[\frac{I_{BS}}{I_0} \frac{r^3}{r_0^2 \lambda} + \frac{I_{BS}}{I_0} \frac{R^4}{R_0^2 A}\right] .$$

The experimental data is a total intensity ratio from the composite surface, where the proportion due to the individual effects is unknown. The geometry of 0° and 10° at 25 cm. range was used so that the results from the wedge as reported in Section B could be separated from the plots with confidence that the remaining information was a result of the rough surface. The lack of any specific shape of the data, Figure 27, that might possibly equate to a simple frequency dependence, is found also in the literature [3,12]; as the backscatter due to sound at low grazing angles is determined by complex processes of multiple scatter and shadowing which have not been adequately described by any theory. The amplitude of this near grazing backscatter in the plots is significant in that it completely masks any diffraction effect of the wedge, which is 5-15 dB less under the same experimental conditions.

This absence of identifiable wedge backscatter now required the experiment to use a model which would reduce the rough surface backscatter relative to wedge diffraction. The previous conclusion of the "smooth" appearance of the wedge with the lead shot covering needed to be reevaluated. The slight roughness of that surface at low grazing angles might produce a combined backscatter with more equitable proportion between the magnitude of the wedge and the rough surface return.

The low grazing, backscatterd signal from the lead shot plate was sampled over different time apertures to see the

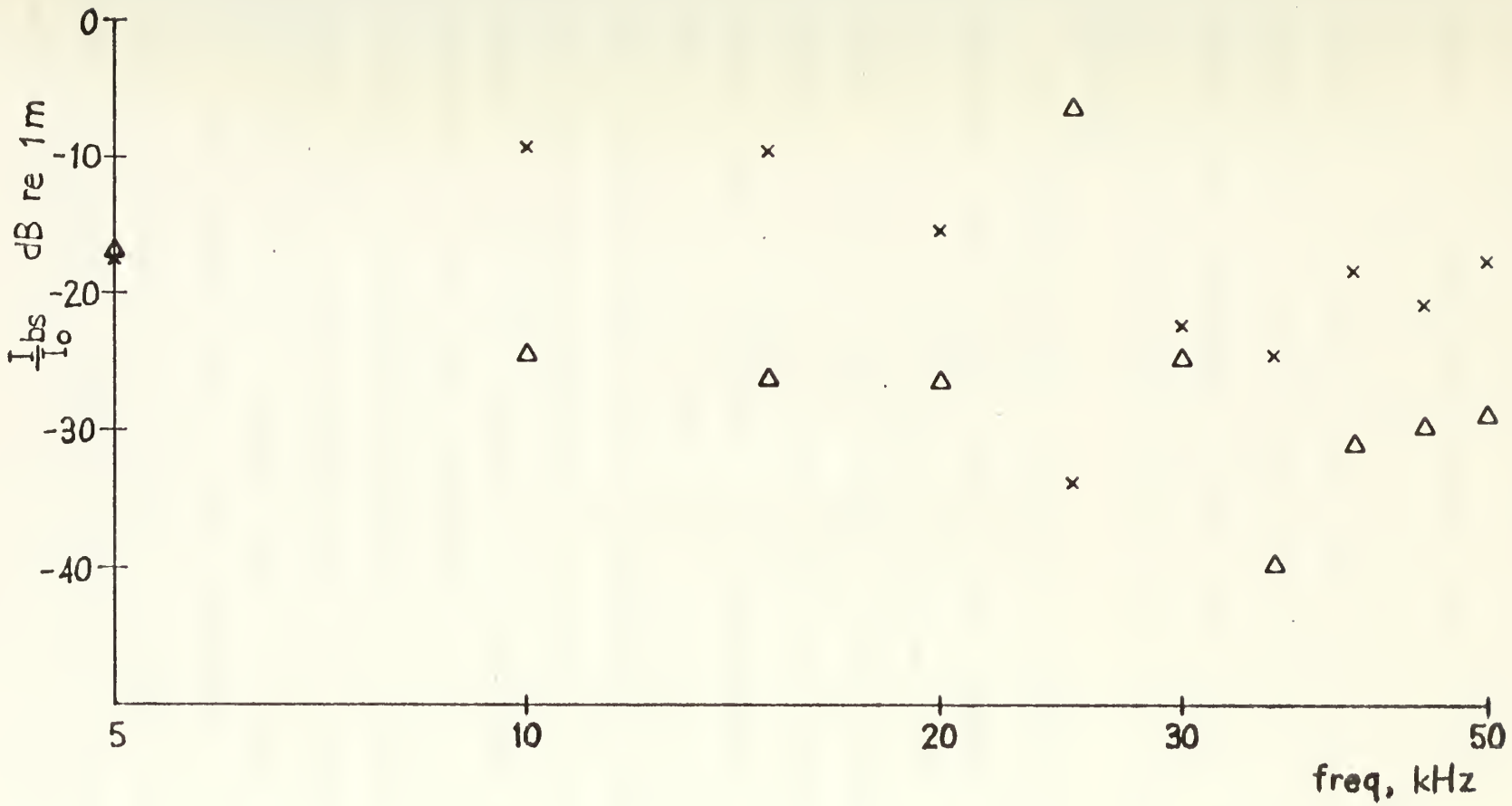

Figure 27. Backscatter from wedge with gravel rough surface, $r = r_0 = 25$ cm, $\theta = \theta_0 = 0°$ (x), $\theta = \theta_0 = 10°$ (Δ).

varying responses of rough surface backscatter or the emergence of the diffracted signal from the crest of the wedge. The least time path (LTP) is the time for sound to travel directly to the crest of the wedge and return. A sampling window prior to the LTP analyzes scattering from the rough surface only; whereas a window that includes the LTP receives the combined scattering effects from the rough surface and the wedge.

An additional data collection run obtained a greater frequency resolution by changing the transmitted frequency of the pulse and the number of samples taken per sampling window. Figures 28 and 29 show a fairly close agreement between the slope of the data and that theoretical slope for the wedge, backscatter. As the grazing angle becomes lower (0° situation, Figure 29), the data tends to diverge from the theoretical line as the magnitude increases from the rough surface backscatter. In the plot of increased frequency resolution (Figure 30), the sampled aperture of rough surface and wedge backscatter (●) follows a pattern of linearly decreasing magnitude with increasing frequency, yet the slope is much greater than the frequency relationship for wedge diffraction alone, which is theoretically $f^{1/2}$ [7]. In Figures 32 and 33, the backscatter from the rough surface alone presents consistent patterns; although once again, no specific frequency dependence relationship can be modeled from the data. The significant feature of this

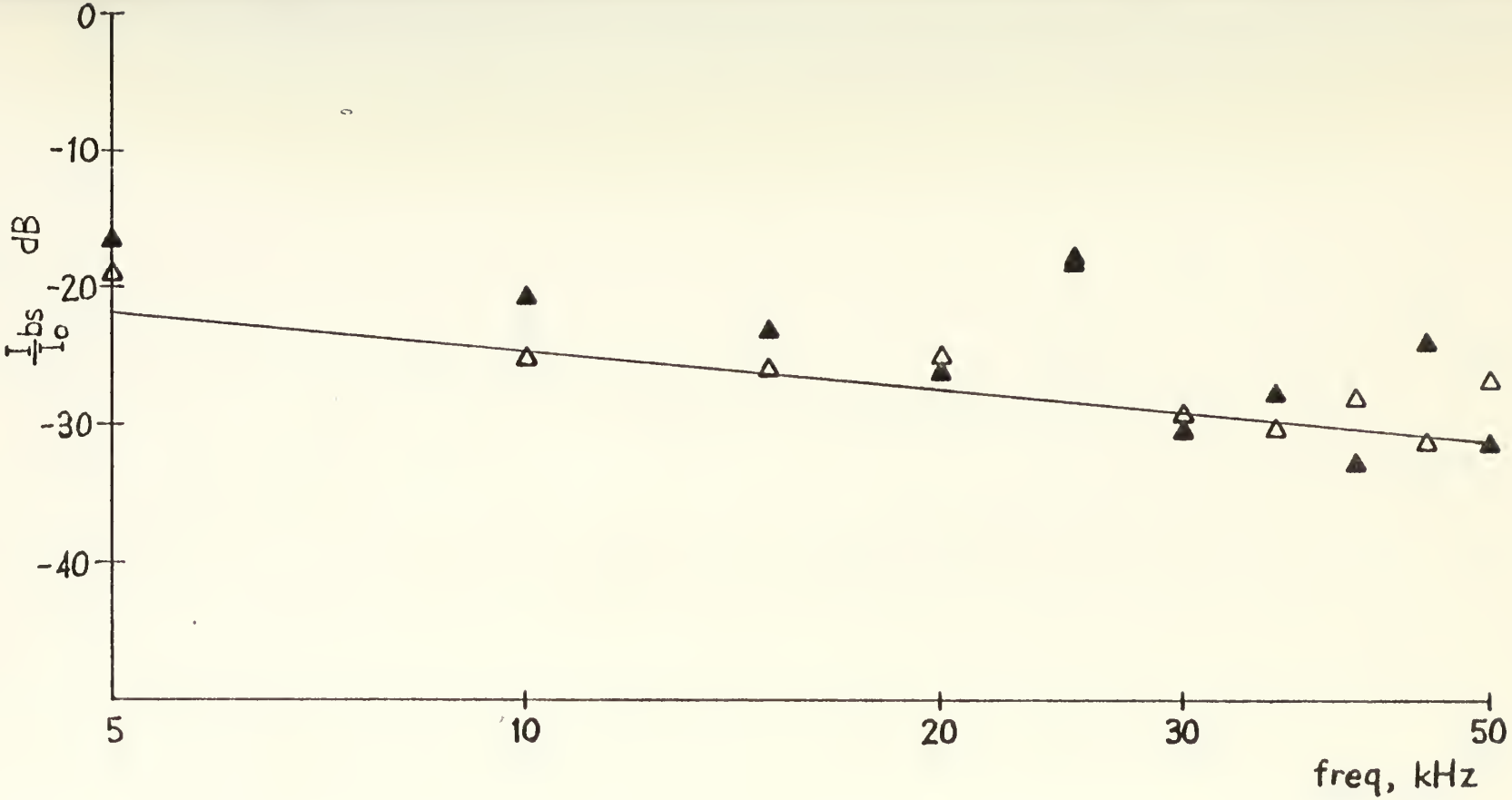

Figure 28. Backscatter from wedge with lead shot surface, $r = r_0 = 25$ cm, $\theta = \theta_0 = 10°$; 1.3 - 1.5 ms (▲), 1.4 - 1.6 ms (Δ), $LTP^0 = 1.4$ ms.

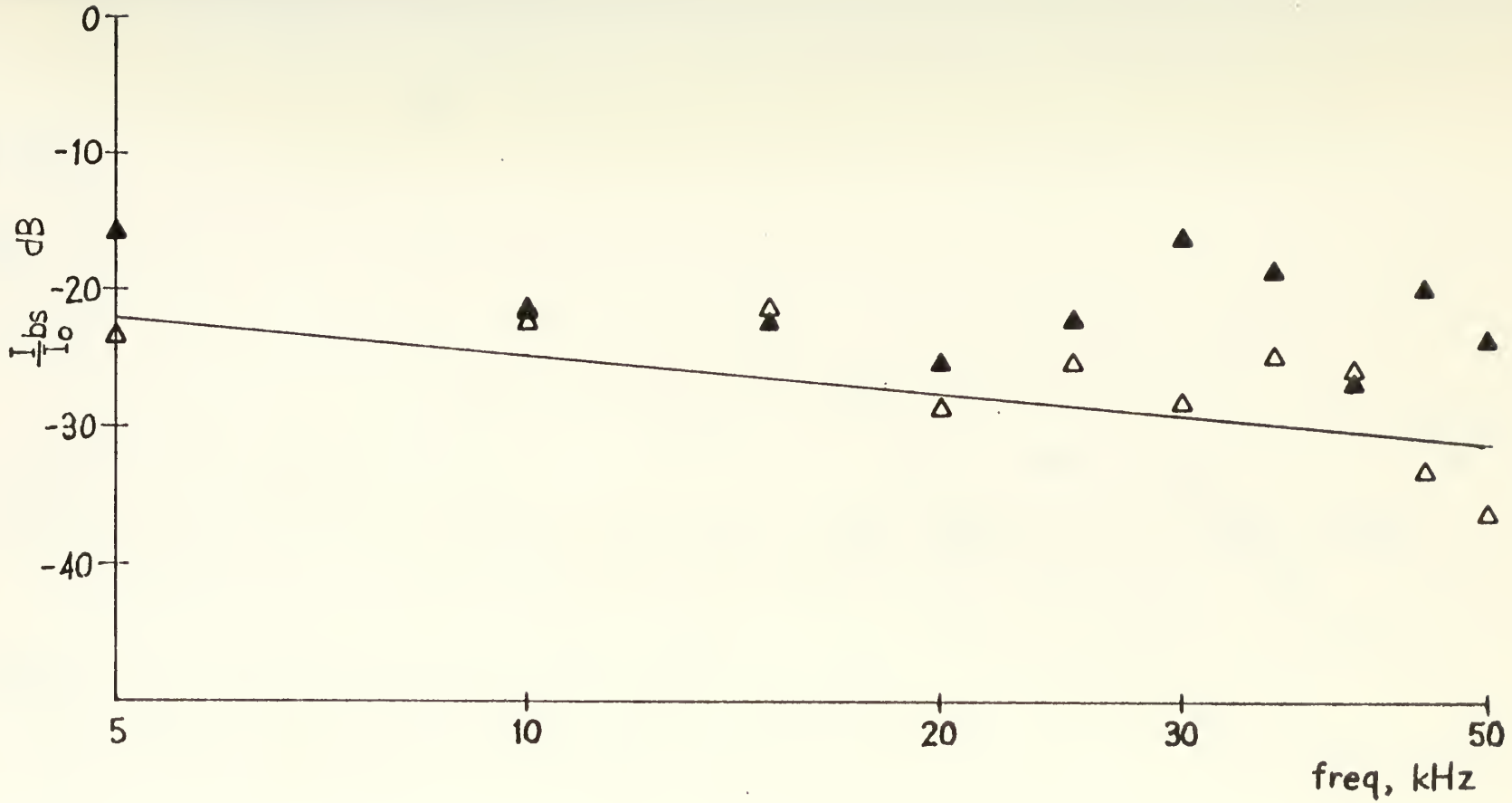

Figure 29. Backscatter from wedge with lead shot surface, $r = r_0 = 25$ cm, $\theta = \theta_0 = 0°$; 1.3 - 1.5 ms (▲), 1.4 - 1.6 ms (△), LTP ≅ 1.4 ms.

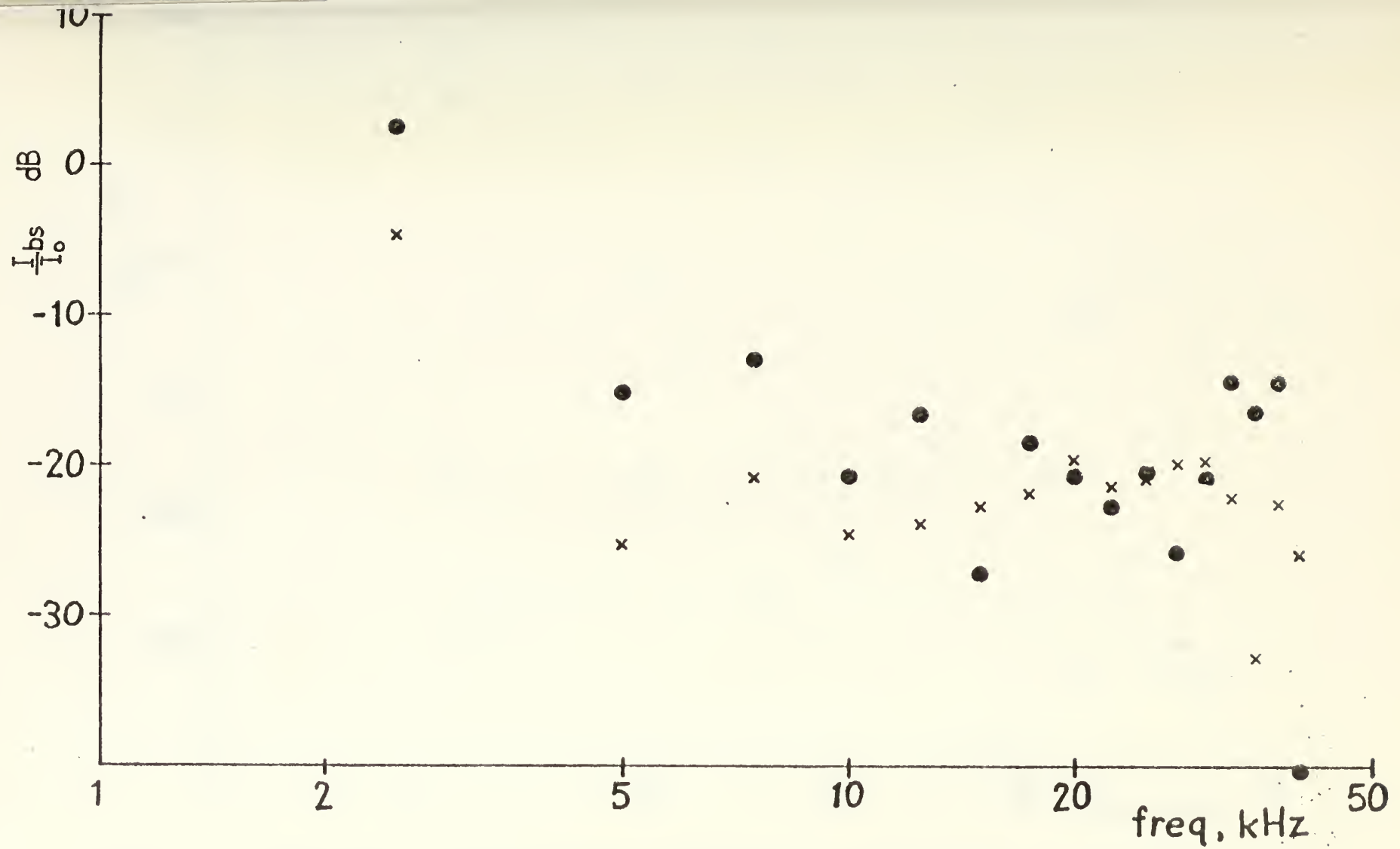

Figure 30. Backscatter from wedge with lead shot surface, $r = r_0 = 25$ cm, $\theta = \theta_0 = 0°$; 1.3 - 1.7 ms (●), 1.5 - 1.9 ms (x), LTP ≅ 1.5 ms.

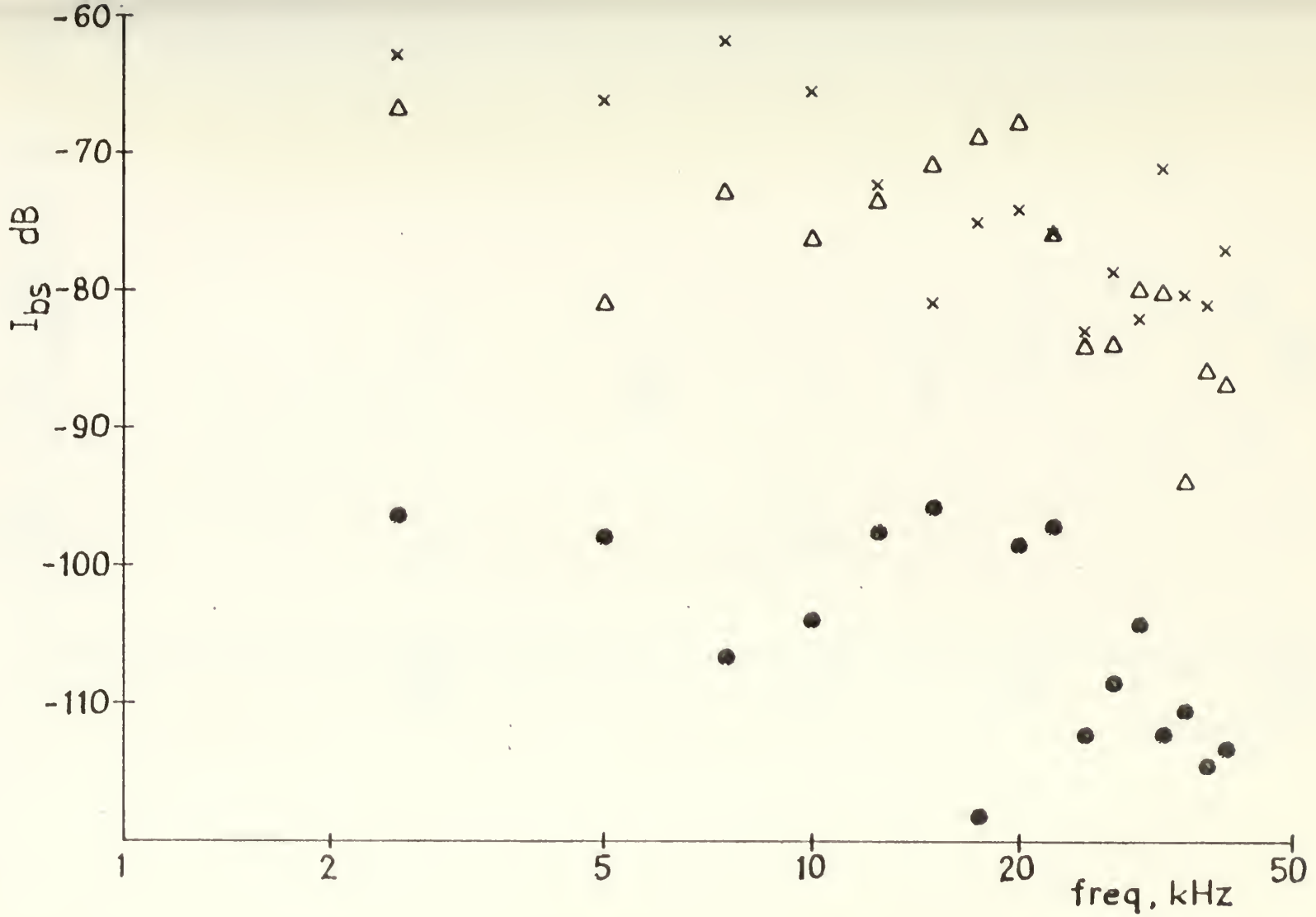

Figure 31. Comparison of wedge backscatter for lead shot surface, $r = r_0 = 25$ cm, $\theta = \theta_0 = 0°$; rough surface only (x), wedge and rough surface (Δ), noise level (●).

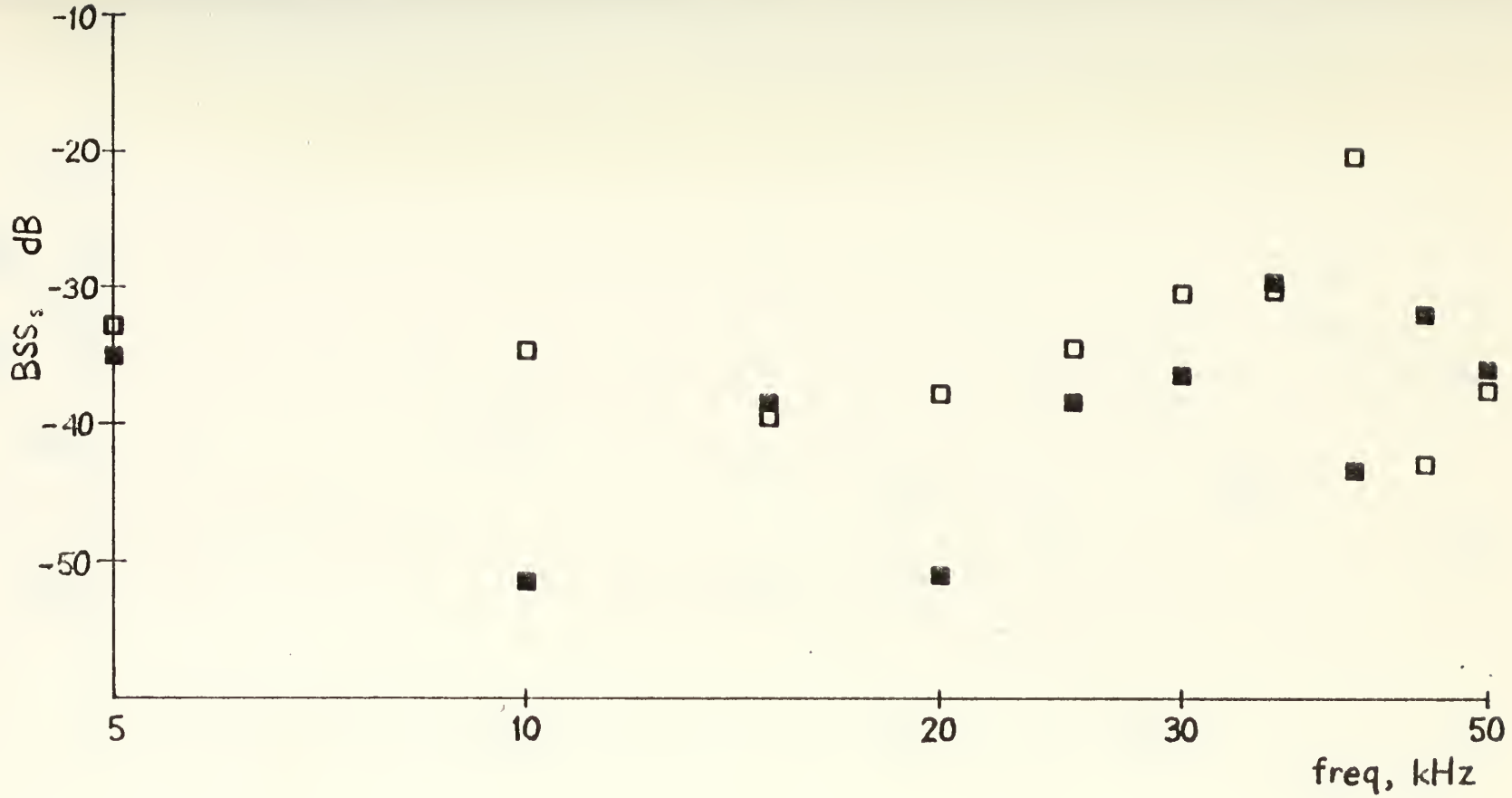

Figure 32. Rough surface backscatter from lead shot surface, $r = r_0 = 25$ cm, $\theta = \theta_0 = 0°$; 1.0 - 1.2 ms (□), 1.2 - 1.4 ms (■), LTP = 1.4 ms.

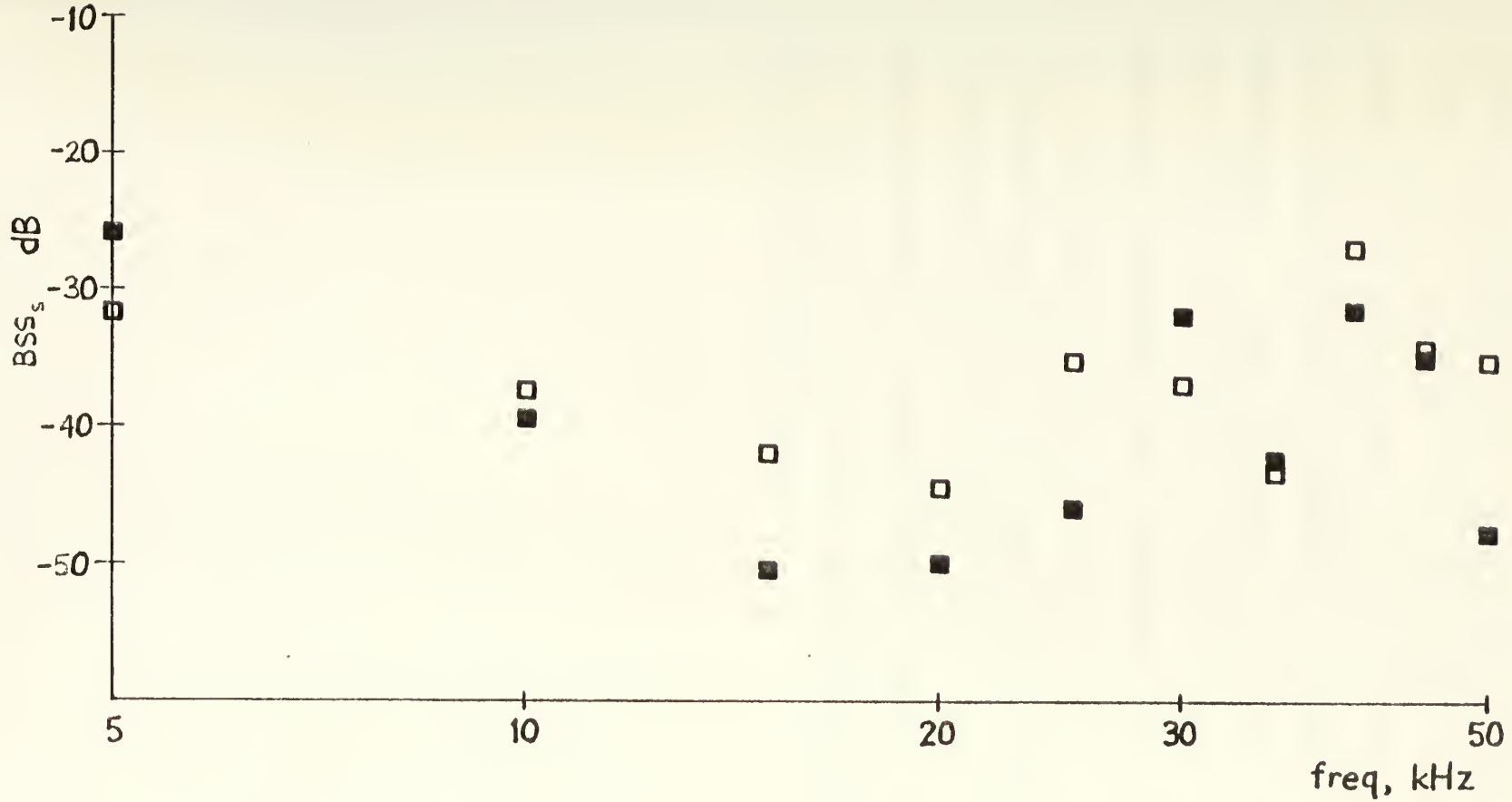

Figure 33. Rough surface backscatter from lead shot surface, $r = r_0 = 25$ cm, $\theta = \theta_0 = 10°$; 1.0 - 1.2 ms (□), 1.2 - 1.4 ms (■), LTP = 1.4 ms.

backscatter effect is the magnitude of the rough surface backscatter. From both the fact that magnitude increases as grazing angle decreases and the relatively greater magnitude of the backscatter as compared to randomly rough surface backscatter in the literature [3,12], the results suggest the boundary wave effects proposed by Tolstoy [6]. Tolstoy describes a boundary wave generated from a rough surface for near grazing incidence and $kh < 1$ (h = separation of roughness elements). The magnitude of backscatter for the experiment suggests the possibility of a large backscattered boundary wave for surfaces of low height roughness, σ/λ, but large slope of the point scattering elements, σ/L, for sound at low grazing angles.

VI. CONCLUSIONS AND RECOMMENDATIONS

Experimental analysis of impulse wave backscatter has been accomplished in the laboratory for various physical models.

The detected return from the shallow change of slope for a plane wedge shows close agreement with the theory proposed by Biot and Tolstoy.

The difference between the actual statistical parameters of the rough surface and those estimated from the spectrum of scattered energy at normal incidence is attributed to the jagged, cusp-like appearance of the surface; that is not accounted for by the theoretical description of the surface.

The inability to positively separate the individual backscatter identities from a composite surface is caused by the disproportion in magnitude between the two effects. The total magnitude in the combined spectrum suggests a large backscattered boundary wave for low grazing angle propagation over interacting steep sloped rough surface elements.

Additional experimental research in this topic could include changes or improvements in the areas of source/receiver selection, physical model design, and theoretical description of rough surfaces.

The ability to find a smaller source/receiver and yet maintain sufficient, detectable output signal and receiver

sensitivity could extend the agreement with theory above 50 kHz. Also, the design of an electronic switching circuit to allow the use of a single microphone for both source and receiver would expand the flexibility in geometry.

A rough surface wedge with a greater wedge slope would increase the backscatter effects from the wedge so that they are not masked by the return from the rough surface.

Further iteration of the mathematical description of the rough surface might more realistically model this natural random surface to the experimental data.

LIST OF REFERENCES

1. Biot, M.A. and Tolstoy, I., "Formulation of Wave Propagation in Infinite Media by Normal Coordinates with an Application to Diffraction", The Journal of the Acoustical Society of America, V. 29, p. 381-391, 1957.

2. Clay, C.S. and Medwin, H., Acoustical Oceanography, Wiley, 1977.

3. Urick, R.J., Principles of Underwater Sound, McGraw-Hill, 1967.

4. Bremhorst, J.H., "Impulse Wave Diffraction by Rigid Wedges and Plates", M.S. Thesis, U.S. Naval Postgraduate School, Monterey, Ca., 1978.

5. Spaulding, R.P., "Physical Modeling of Sound Shadowing by Seamounts", M.S. Thesis, U.S. Naval Postgraduate School, Monterey, Ca., 1979.

6. Tolstoy, I., Wave Propagation, McGraw-Hill, 1973.

7. Medwin, H., "Shadowing by Finite Barriers", The Journal of the Acoustical Society of America, in press for publication.

8. Beckmann, P. and Spizzichino, A., The Scattering of Electromagnetic Waves from Rough Surfaces, MacMillan, 1963.

9. Sessler, G.M. and West, J.E., "Electret Transducers: A Review", The Journal of the Acoustical Society of America, V. 53, p. 1589-1599, June 1973.

10. Frederiksen, E., "Condenser Microphones Used As Sound Sources", Bruel & Kjaer Technical Review, No. 3, 1977.

11. Jordan, E., preparation for M.S. Thesis, U.S. Naval Postgraduate School, Monterey, Ca., 1980.

12. Medwin, H., "Scattering From the Sea Surface", from Stephens, Underwater Acoustics, Wiley, 1970.

INITIAL DISTRIBUTION LIST

		No. Copies
1.	Defense Documentation Center Cameron Station Alexandria, Virginia 22314	2
2.	Library, Code 0142 Naval Postgraduate School Monterey, California 93940	2
3.	Department Chairman, Code 61 Department of Physics and Chemistry Naval Postgraduate School Monterey, California 93940	2
4.	Professor H. Medwin, Code 61Md Department of Physics and Chemistry Naval Postgraduate School Monterey, California 93940	3
5.	Professor O.B. Wilson, Code 61Wl Department of Physics and Chemistry Naval Postgraduate School Monterey, California 93940	1
6.	Lt. Wilson B. Decker, USN COMFAIRKEFLAVIK, Box 2 FPO New YOrk, N.Y. 09571	1
7.	Office of Naval Research Arlington, Virginia 22217	
	Attn: Code 480	3
	Attn: Dr. M. McKisic (Code 486)	1
	Attn: Code 460	1
	Attn: Code 102-05	1

Thesis 191198
D2344 Decker
c.1 Backscatter from a composite rough surface.